Journal Pre-proof

Discovery and optimization of withangulatin A derivatives as novel glutaminase 1 inhibitors for the treatment of triple-negative breast cancer

Wu-Xi Zhou, Chen Chen, Xiao-Qin Liu, Ying Li, Yao-Lan Lin, Xiu-Tao Wu, Ling-Yi Kong, Jian-Guang Luo

PII: S0223-5234(20)30952-1

DOI: https://doi.org/10.1016/j.ejmech.2020.112980

Reference: EJMECH 112980

To appear in: *European Journal of Medicinal Chemistry*

Received Date: 24 September 2020

Revised Date: 25 October 2020

Accepted Date: 27 October 2020

Please cite this article as: W.-X. Zhou, C. Chen, X.-Q. Liu, Y. Li, Y.-L. Lin, X.-T. Wu, L.-Y. Kong, J.-G. Luo, Discovery and optimization of withangulatin A derivatives as novel glutaminase 1 inhibitors for the treatment of triple-negative breast cancer, *European Journal of Medicinal Chemistry*, https://doi.org/10.1016/j.ejmech.2020.112980.

Graphical abstract

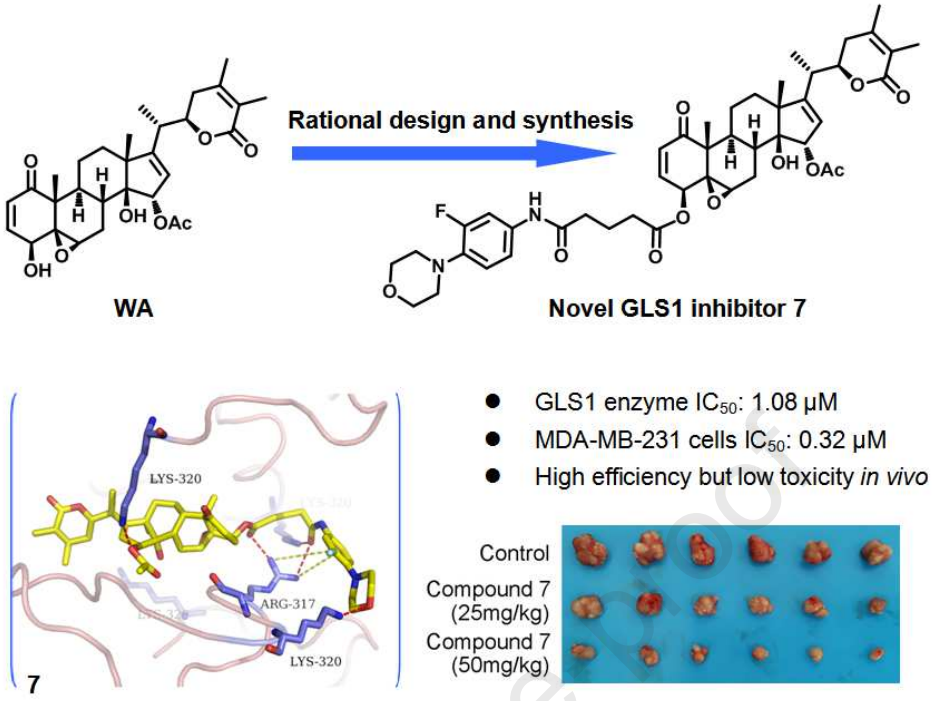

Discovery and optimization of withangulatin A derivatives as novel glutaminase 1 inhibitors for the treatment of triple-negative breast cancer

Wu-Xi Zhou [a, #], Chen Chen [a, #], Xiao-Qin Liu [a], Ying Li [a], Yao-Lan Lin [a], Xiu-Tao Wu [a], Ling-Yi Kong [a, *], Jian-Guang Luo [a, *]

[a] *State Key Laboratory of Natural Medicines, Jiangsu Key Laboratory of Bioactive Natural Product Research, School of Traditional Chinese Pharmacy, China Pharmaceutical University, 24 Tong Jia Xiang, Nanjing, 210009, PR China*

[#] *Authors contributed equally*

** Corresponding author: lykong@cpu.edu.cn (L.-Y. Kong), luojg@cpu.edu.cn (J.-G. Luo)*

Abstract

To develop novel GLS1 inhibitors as effective therapeutic agents for triple-negative breast cancer (TNBC), 25 derivatives were synthesized from the natural inhibitor withangulatin A (IC_{50} = 18.2 μM). Bioassay optimization identified a novel and selective GLS1 inhibitor **7** (IC_{50} = 1.08 μM). In MDA-MB-231 cells, **7** diminished cellular glutamate levels by blocking glutaminolysis pathway, further triggering the generation of reactive oxygen species to induce caspase-dependent apoptosis. Molecular docking indicated that **7** interacted with a new reacting site of allosteric binding pocket by forming various interactions in GLS1. The intraperitoneal administration of **7** at a dose of 50 mg/kg exhibited remarkable therapeutic effects and no apparent toxicity in the MDA-MB-231 xenograft model, indicating its potential as a novel GLS1 inhibitor for treatment of TNBC.

Keywords: Withangulatin A derivatives; GLS1 inhibitors; Molecular docking; Antitumor;

TNBC

1. Introduction

Glutaminolysis is one of the main metabolic pathways in cancer cells to produce energy to meet the demands of their rapid and sustained growth [1-3]. Glutamine is hydrolyzed by glutaminase 1 (GLS1) into glutamate, which is further converted into α-ketoglutarate by glutamate dehydrogenase. The α-ketoglutarate produced in this process can enter the tricarboxylic acid cycle to supply cellular nutrients [4-6]. Moreover, glutaminolysis pathway is essential for cellular reactive oxygen species (ROS) homeostasis [5]. Owing to the addiction of many cancer cells to glutamine, blocking glutaminolysis was considered to be an attractive strategy for cancer therapy [7-9].

GLS1, as a key metabolic enzyme, controls the first step in the glutaminolysis pathway. Suppression of the expressed form of GLS1 has antitumor activity across many tumor types, including glioma, pancreatic, lymphoma, breast and renal cancers [10-14]. Notably, GLS1 expression level is associated with high grade and metastatic breast cancer [15]. In particular, TNBC cells have high levels of GLS1 as well as an increased uptake of glutamine to supply the cells with intermediates to meet the TCA cycle [16-18]. Currently, the treatment of TNBC usually relies on chemotherapy. Several studies have aimed at the development of novel chemotherapies [19-22], while there is still a lack of satisfactory therapeutic agents in the market. In recent years, TNBC cells are reported to be used for screening antitumor activity of GLS1 inhibitors *in vitro*, of which the most commonly used is MDA-MB-231 [23]. These observations highlight the critical connection between breast carcinoma and GLS1 and suggest that GLS1 is a potential therapeutic target for anti-TNBC drug discovery and development [8, 24-26]. Although the potential benefits of GLS1 inhibition have been recognized for many years, small molecule GLS1 inhibitors were relatively scarce and

merely chemically synthesized derivatives, DON, BPTES and CB-839, were available to date [27, 28]. Nevertheless, some shortcomings, such as nonspecificity, low solubility and moderate potency, may limit their pharmacological applications [29, 30].

Natural products are important sources for the discovery and development of novel anticancer drugs [31]. Recently, we found that withangulatin A (**WA**, **Fig. 1**) with a withanolide scaffold isolated from *Physalin* species exhibited potent anticancer activities [32-35]. In several cancer models, **WA** has been proven to inhibit tumor metastasis, reduce cell proliferation, and induce cell apoptosis, which makes **WA** a promising drug for cancer therapy [36, 37]. More interestingly, **WA** was found to have a moderate GLS1 inhibitory activity (IC_{50} = 18.2 μM). Structure-based optimizations based on **WA** lead to the discovery of a potent GLS1 inhibitor **7** with IC_{50} = 1.08 μM and favorable physicochemical properties. In particular, this compound exhibited a different binding site from traditional GLS1 inhibitors. Intraperitoneal administration of **7** exhibited remarkable therapeutic effects and no apparent toxicity in the MDA-MB-231 xenograft model, indicating its potential as a novel GLS1 inhibitor for treatment of TNBC.

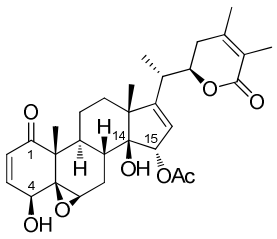

Fig. 1. Structure of withangulatin A (**WA**)

2. Results and discussion

*2.1. Design of GLS1 inhibitors based on **WA***

WA was found to have moderate GLS1 inhibitory activity (IC_{50} = 18.2 μM). Further

efforts focus on structural modifications, and optimization of this scaffold are still needed today. In the search for novel antitumor GLS1 inhibitors with higher potency, we designed a series of **WA** derivatives in which a 4-hydroxyl group was modified with different types of substituents derived from small molecule GLS1 inhibitors via different linkers (**Fig. 2**).

BPTES, as the first reported small molecule GLS1 allosteric inhibitor, showed potent GLS1 inhibitory activity (IC_{50} = 3.3 μM) [38-41]. The structure of BPTES (**Fig. 2**) consists of two exactly equivalent parts including thiadiazole, amide, and phenyl groups. This structural characteristic allows it to easily interact with GLS1 allosteric pocket and effectively trap GLS1 as an inactive tetramer [42]. On the basis of the scaffold of BPTES, some derivatives were synthesized for the purposed of improving the GLS1 inhibitory activity and structure-activity relationship (SAR) data were presented [43, 44] The amide groups play an important role in binding, while the terminal thiadiazole can be replaced by a variety of amide groups while retaining the inhibitory activity of GLS1. In addition, the phenyl groups can be modified without losing the GLS1 inhibitory activity [44]. Thus, substituents containing these binding groups or their analogues were first introduced to **WA** to improve the enzymatic inhibition activities and cell inhibition activities.

WA showed the presence of two hydroxyl and an α, β-unsaturated ketone functions (**Fig. 1**). For **WA** analogs, the OH group at the C-4 position was utilized to incorporate the ester linkage, since the reactivity of the hydroxyl group at C-4 is much higher than that at C-14 [45]. Previous studies found that the enone moiety of **WA** is essential for its anticancer activity and that the acetylation of 4-hydroxyl could lead to improvement of activity [46]. However, the introduction of large steric hindered groups into 4-hydroxyl of **WA** resulted in a loss of the potency. Thus, different linkers with varying structure and length were evaluated as survey of the potential chemical space. In addition, these linkers contain two carbonyl

groups connected to the substituents via an amide linkage, which was expected to be susceptible to binding with GLS1 allosteric pocket. Therefore, in the present study, different types of substituents derived from BPTES were introduced to the 4-hydroxyl of **WA** by different linkers leading to the discovery of a novel molecule **7** with enhanced GLS1 inhibitory activity as the candidate for TNBC therapy.

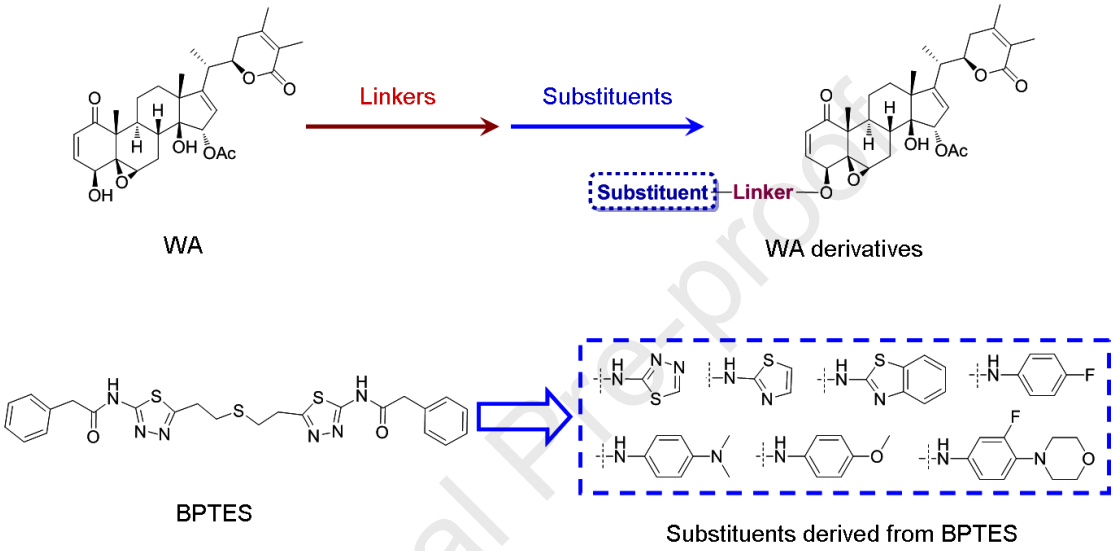

Fig. 2. Design of GLS1 inhibitors based on **WA** and BPTES binding groups.

2.2. Chemistry

The synthetic routes to the intermediates **a-d** and the **WA** derivatives **1-25** are shown in **Schemes 1** and **2** and detailed in the experimental section. Initially, the 4-hydroxyl group in **WA** was acylated with glutaric anhydride, succinic anhydride, maleic anhydride or phthalic anhydride in dry DCM under reflux conditions to give intermediates **a**, **b** or **c**, respectively (**Scheme 1**). Besides, 4-(2-fluoro-4-nitrophenyl)morpholine was prepared with 3,4-difluoronitrobenzene and morpholine in DMSO, followed by treatment with 10% Pd-C in the presence of hydrogen in ethyl acetate to produce intermediate **d** (**Scheme 2**). Subsequently, the appropriate substituents were conjugated with **a**, **b** or **c** in the presence of catalyst HOBt•H_2O, EDCI•HCl and pyridine in DMF at room temperature to obtain the target

compounds **1-21** (**Scheme 1**). To validate that the enone moiety of **WA** is essential for activity, compounds **22-25** were identified by Michael addition (**Scheme 1**).

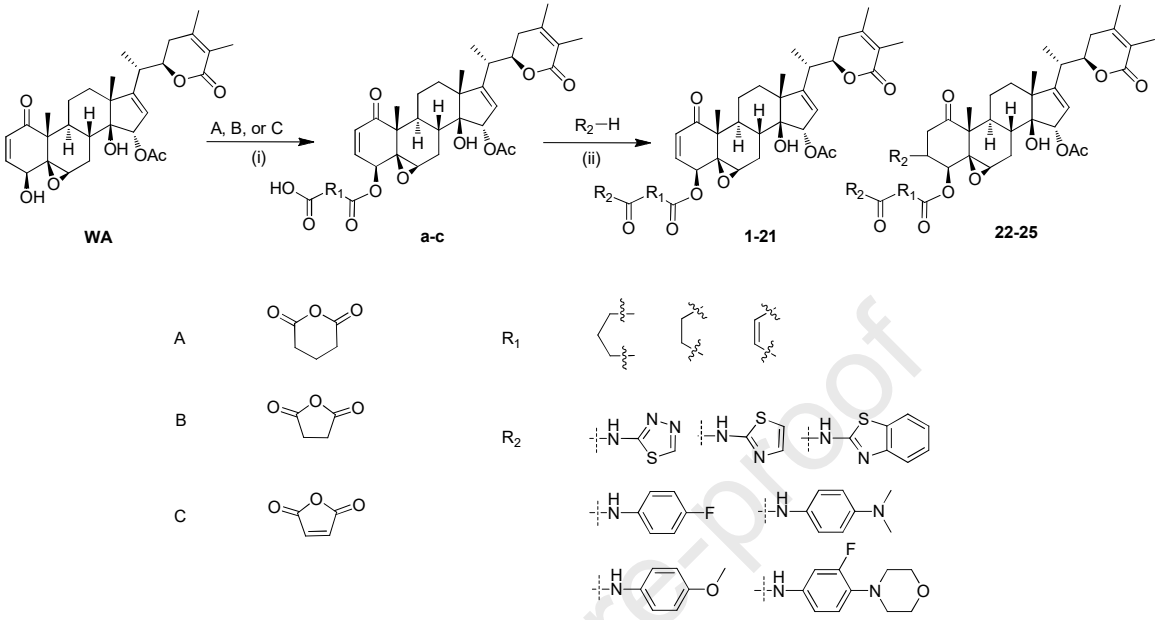

Scheme 1. Synthesis of **WA** derivatives **1-25**. Reagents and conditions: (i) TEA, DCM, reflux, 40-72 h. (ii) HOBt•H_2O, EDCI•HCl, pyridine, DMF, rt, 15-48 h.

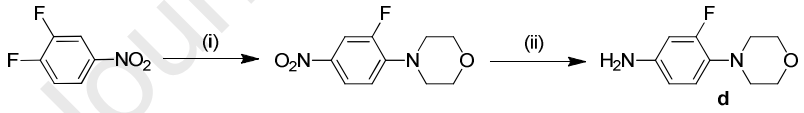

Scheme 2. Synthesis of intermediate d. Reagents and conditions: (i) Morpholine, KH_2PO_4, DMSO, 60 °C, 24 h. (ii) 10% Pd-C/H_2, EtOAc, rt, 6 h.

2.3. Anti-proliferative activity in vitro

MDA-MB-231 cells, a TNBC cells, have high expression of GLS1 [16-18]. These cells are reported to be used for screening antitumor activity of GLS1 inhibitors *in vitro* [23]. Therefore, we primarily began our research by screening the inhibitory activities of **WA** derivatives in MDA-MB-231. The cytotoxicity of **WA** derivatives against MDA-MB-231 cell line was tested, and the IC_{50} values and the maximum inhibition ratio were summarized in

Table 1. Obviously, the current data suggest that the hydroxyl substitutions at the C-4 atom are crucial; when hydroxyl at the C-4 atom is substituted (compounds **1**-**21**), most derivatives demonstrate better anti-proliferative activity than that of **WA**. Meanwhile, the derivatives, with addition at the C-3 (compounds **22-25**), revealed no anti-proliferative activity, which demonstrated that enone moiety of **WA** was essential for inhibitory activity [46]. As shown in **Table 1**, compounds **1**, **2**, **8**, **9**, **15** and **16** containing either a thiadiazole ring or a thiazole ring did not improve activity, while the introduction of benzothiazole displayed the highest inhibition (IC_{50} = 0.67±0.03 μM) for compound **3**. In addition, the heterocyclic ring was replaced by a phenyl ring that could be useful to improve the inhibitory activity (compounds **4, 11** and **18**). Therefore, the phenyl ring of the substituents was maintained, and **WA** derivatives with phenyl ring were prioritized. Subsequently, the introduction of an N, N-dimethylaniline in compounds **5**, **12** and **19** improved inhibitory activity. This was also observed with the electron-donating methoxy group in compounds **6**, **13** and **20**. Interestingly, morpholine saturated ring substituent derivatives (**7**, **14** and **21**) in which phenyl ring, nitrogen and oxygen were included exhibited potent anti-proliferative activities.

To further validate our design strategy of improving inhibition activities, three linkers were selected. When the chain length of the linker region was five carbon atoms, compound **7** exhibited strongest inhibitory activity. However, compounds **14** and **21**, which contained four carbon atoms or an olefinic bond in linker region, reduced inhibitory activities. These results suggested that the flexibility of the linker determining the spatial orientation of substituent portion was important for the inhibitory activities. Moreover, these linkers contain two carbonyl groups connected to the substituents via an amide linkage, which might provide a binding group for protein-ligand interactions, but the intermediates with a carboxyl (compounds **a**-**c**) revealed no inhibitory activity. Based on that, we identified a derivative **7** with a substituent 3-fluoro-4-morpholinoaniline which dramatically improved the potency

(IC_{50} = 0.32 ± 0.003 μM). Almost complete inhibition was achieved by **7** in a biochemical assay compared with **WA** and BPTES (**Table 1**), which indicated good efficacy in a cell-based assay.

2.4. Inhibition of GLS1 activity

Based on potent inhibition effects in MDA-MB-231 cells, the inhibition effects on GLS1 were necessary to be evaluated to further characterize our products. The inhibition effects of **WA** derivatives, **WA** and BPTES on the GLS1 activity was investigated using the GLS1 inhibitor screening assay kit. The GLS1 inhibitor screening assay kit is designed to measure the hydrolase activity of GLS1 for screening and profiling applications. All the synthesized derivatives were initially tested at a concentration of 10 μM for their potency to inhibit GLS1 (**Table 1**). Among the active compounds showing greater than 50% inhibition, the one with the highest inhibition rate was selected for IC_{50} measurement under these screening conditions and compared with **WA** and BPTES. The results are shown in **Table 1**. Excitingly, all of the three compounds showed increased inhibitory activities on GLS1, especially **7** with an IC_{50} of 1.08 μM with improved efficacy of about 20-fold than that of **WA** (IC_{50}, 18.2 μM). It was more potent compared with BPTES with IC_{50} of 4.57 μM (**Table 1**). To date, **7** is the best GLS1 inhibitor in our studies, which validated our structure modification strategy.

Taken together, when the linker is glutaric acid, substituent is a phenyl ring with fluorine, nitrogen and oxygen, and hydroxyl substitutions at the C-4 atom of **WA**, the enzyme inhibitory activity and cytotoxic activity are improved. The most potent compound **7** exhibited approximately 20 times stronger cytotoxicity and 20 times higher inhibitory activity of GLS1 than those of **WA**, respectively. Since topological polar surface area (tPSA) and LogP values have potential impact on the ability of cell penetration, we calculated those values of **7**. According to the calculated values, compound **7** had better LogP and other

physicochemical properties than **WA** itself (**Table S1**), and deserved further biological activity assays and pharmacological mechanistic study as a new antitumor candidate agent.

Table 1. Inhibition of GLS1 enzyme and MDA-MB-231 cells by **WA** derivatives.

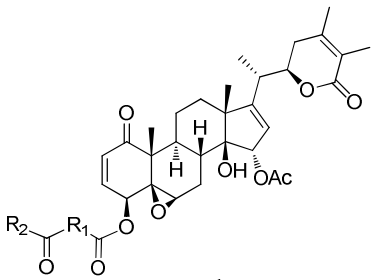

a-c and **1-21**

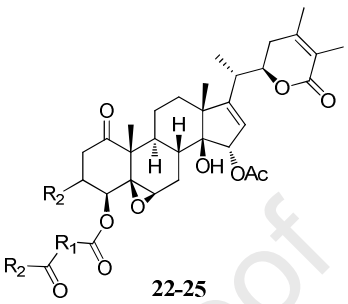

22-25

Compd	R_1	R_2	GLS1		MDA-MB-231	
			Inhibition (%) [a]	IC_{50} (μM) [b]	IC_{50} (μM) [b]	Max-INH (%) [c]
a	$-CH_2CH_2CH_2-$	-OH	<50	-	>50	-
b	$-CH_2CH_2-$	-OH	<50	-	>50	-
c	-CH=CH-	-OH	<50	-	>50	-
1	$-CH_2CH_2CH_2-$	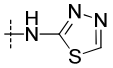	<50	-	2.17±0.07	71.6±1.5
2	$-CH_2CH_2CH_2-$	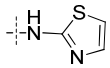	<50	-	1.00±0.06	84.8±2.4
3	$-CH_2CH_2CH_2-$	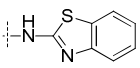	<50	-	0.67±0.03	94.1±0.6
4	$-CH_2CH_2CH_2-$	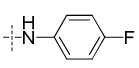	<50	-	0.49±0.02	95.4±0.3
5	$-CH_2CH_2CH_2-$	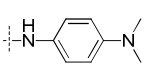	51.76±0.88	-	1.07±0.05	92.6±1.9
6	$-CH_2CH_2CH_2-$	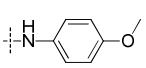	56.30±2.78	-	0.44±0.006	92.9±0.5

7	-$CH_2CH_2CH_2$-	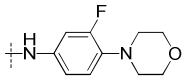	87.20±5.06	1.08±0.02	0.32±0.003	95.2±0.4
8	-CH_2CH_2-	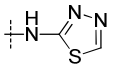	<50	-	8.07±0.35	77.5±1.4
9	-CH_2CH_2-	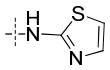	<50	-	2.06±0.09	79.6±2.5
10	-CH_2CH_2-	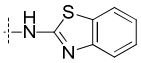	<50	-	3.50±0.16	79.5±1.2
11	-CH_2CH_2-	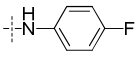	<50	-	1.87±0.11	80.4±3.4
12	-CH_2CH_2-	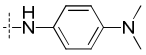	<50	-	1.62±0.09	83.3±1.2
13	-CH_2CH_2-	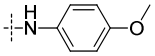	<50	-	1.02±0.04	82.9±3.8
14	-CH_2CH_2-	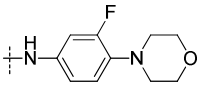	53.45±3.38	-	1.66±0.07	80.9±0.9
15	-CH=CH-	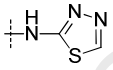	<50	-	8.45±0.45	65.4±2.5
16	-CH=CH-	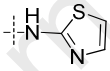	<50	-	1.83±0.09	88.4±1.1
17	-CH=CH-	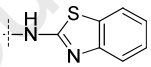	<50	-	>50	0
18	-CH=CH-	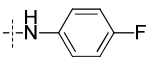	<50	-	1.32±0.03	88.9±1.6
19	-CH=CH-	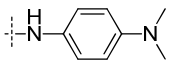	<50	-	1.56±0.05	72.1±2.6
20	-CH=CH-	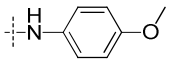	51.58±1.89	-	0.79±0.009	94.1±0.5
21	-CH=CH-	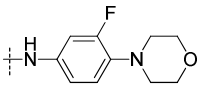	52.44±3.89	-	1.38±0.005	90.8±1.2
22	-$CH_2CH_2CH_2$-	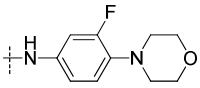	<50	-	>50	0
23	-$CH_2CH_2CH_2$-	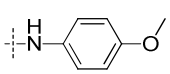	<50	-	>50	0

24	-CH_2CH_2-	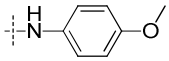	<50	-	>50	0
25	-CH=CH-	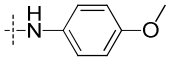	<50	-	>50	0
WA			41.40±0.99	18.20±0.56	6.34±0.17	74.7±1.6
BPTES [d]			52.35±1.62	4.57±0.09	9.08±0.27	68.5±1.3

[a] In vitro inhibition of compound concentration of 10 μM in GLS1. [b] The concentration of an inhibitor where the response is reduced by half. [c] In vitro maximal inhibition in MDA-MB-231 cell lines. All values are the means ± SD of four independent experiments. [d] Positive control.

2.5. Cell viability and clonogenicity

To investigate the ability of **7** to induce cell death, MDA-MB-231 cells were cultured with different concentrations of **7**, and the cell viability was measured. The results are shown in **Fig. 3A**. The results suggest that **7** significantly decreased the viability of MDA-MB-231 cells in a dose-dependent manner, which is more potent than that of **WA**. We also examined the long-term effect on the proliferation of MDA-MB-231 cells under treatment of **7** by colony formation assay (**Fig. 3B** and **C**). Consistently, the proliferation of MDA-MB-231 cells was notably inhibited by **7**, and compared with **WA**, it is more evident.

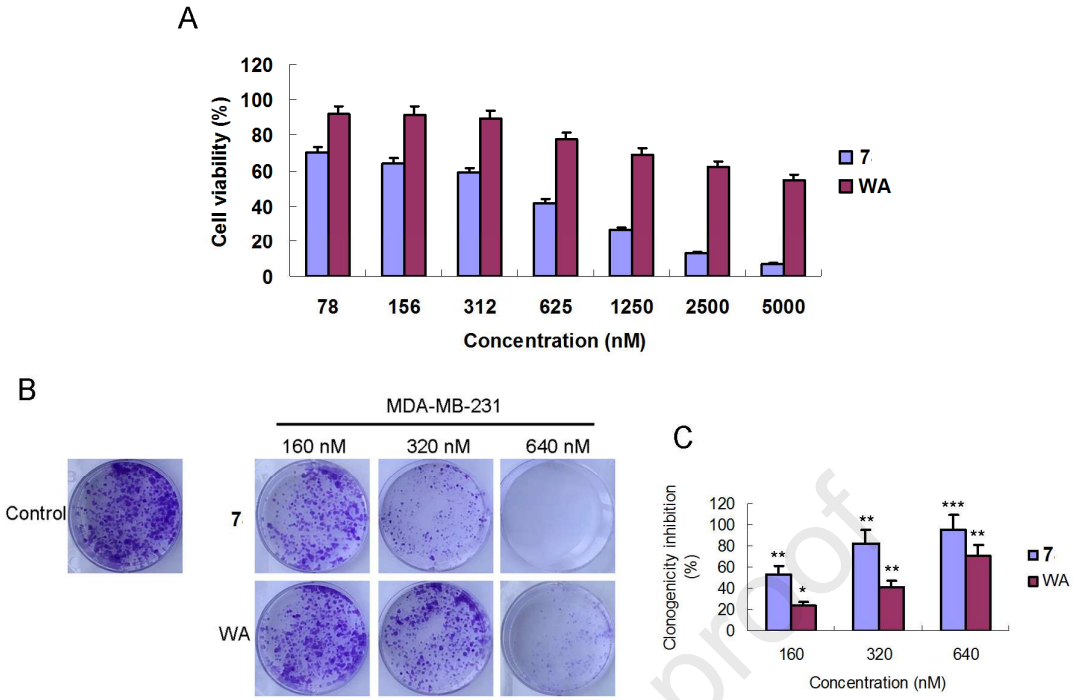

Fig. 3. Compound **7** inhibits the proliferation of MDA-MB-231 cells. (A) MDA-MB-231 cells were treated with the different concentrations of **7** or **WA** for 24 hours and cell viability was detected by MTT assay. (B) Compound **7** inhibited colony formation of MDA-MB-231 cells. MDA-MB-231 cells were treated with the different concentration of **7** or **WA** for 24 hours. After treatment, the cells were seeded into 6-well plates for two weeks. (C) The clonogenicity inhibition was presented as percentage relative to the vehicle treatment. Data represent the means ± SD (n = 4), *P < 0.05, **P < 0.01, ***P < 0.001, compared with control group.

2.6. Compound 7 induced apoptosis in MDA-MB-231 cells

To validate the decreased viability of **7**-treated cells is attributed to apoptosis, MDA-MB-231 cells were treated with **7** and apoptotic changes were tested. Annexin V/PI double-stained assay measured with flow cytometry showed that **7** significantly elevated the total number of Annexin V/ PI double-stained (early apoptosis and late apoptosis) cells (**Fig. 4A and B**). Furthermore, western blotting analysis suggested that **7** caused a dose-dependent increase in the expression of cleaved caspase-3 and cleaved caspase-9 (**Fig. 4C and D**), which are widely used apoptotic marker [47]. These data indicated that **7** induced apoptosis

and that it was via a caspase-dependent pathway in GLS1 high-expressing MDA-MB-231 cell line.

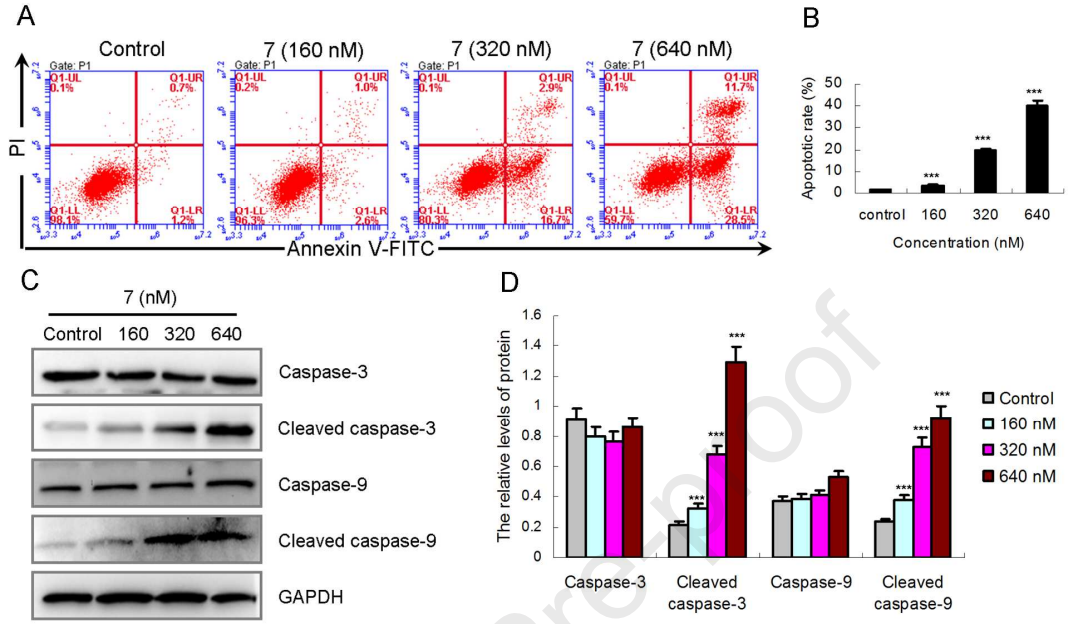

Fig. 4. Compound **7** induces apoptosis of MDA-MB-231 cells. (A) MDA-MB-231 cells were treated with different concentrations of **7** for 12 h, and then fixed and stained with Annexin V-FITC/PI and analyzed by flow cytometry; Acquisition of Annexin V-FITC and PI data are presented as a percentage (%) in each quadrant. The early and late apoptotic cells are presented in the lower and upper right quadrant, respectively. (B) And the apoptosis rate was quantitated. Data represent the means ± SD (n = 4), ***P < 0.001, compared with control group. (C) Western blotting analysis of **7** in MDA-MB-231 cells. MDA-MB-231 cells were treated with the different concentrations of **7** for 12 h; then the protein expression of caspase-3, cleaved caspase-3, caspase-9, and cleaved caspase-9 were evaluated by western blotting; GAPDH was used as an internal control. (D) Quantitative analysis. Data represent the means ± SD (n = 4), ***P < 0.001, compared with control group.

*2.7. Compound **7** inhibited cellular glutamate production*

Cellular Glutamate was detected using Amplex® Red Glutamic Acid Assay Kit (Invitrogen). Experiments are carried out following the manufacturer's instructions. In the assay, compound **7** was found to diminish glutamate production in a dose-dependent manner

in MDA-MB-231 cells (**Fig. 5**). In addition, compared with **WA**, **7** was more potent in reducing cellular glutamate production. These results demonstrated that **7** could effectively inhibit GLS1 and block the glutamine hydrolysis pathway, which could lead to cell death.

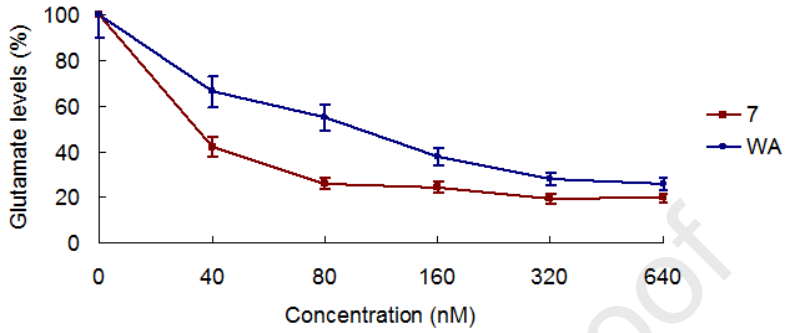

Fig. 5. Effect of compound **7** and **WA** on the cellular glutamate levels of MDA-MB-231 cells.

*2.8. Compound **7** induced reactive oxygen species (ROS) generation*

Cell signals mediated by reactive oxygen species (ROS) can promote tumor development at a certain physiological level [48], but when the level is too high, reactive oxygen can cause great damage to macromolecules in cells [49]. However, tumor cells can directly control ROS levels through molecules produced by the glutamine metabolism pathway, preventing high levels of ROS from causing chromosomal instability [50]. Hence, glutamine metabolism is vital for cellular ROS homeostasis. The ROS level was tested using a fluorogenic dye (DCFH-DA) by fluorescence microscopy and flow cytometry. As shown in **Fig. 6A** and **B**, **7** could significantly enhance intracellular ROS levels in a dose-dependent manner in MDA-MB-231 cells, which was more potent than **WA**. In particular, as shown in **Fig. 6C**, it was clear that significant fluorescence intensity of MDA-MB-231 cells confirmed that **7** was able to achieve superior properties on cellular internalization with the highest level of fluorescence intensity detected at 640 nM in comparison with that of **WA**. These results

proved that **7** as a GLS1 inhibitor could effectively block the glutamine hydrolysis pathway, further triggering the generation of ROS.

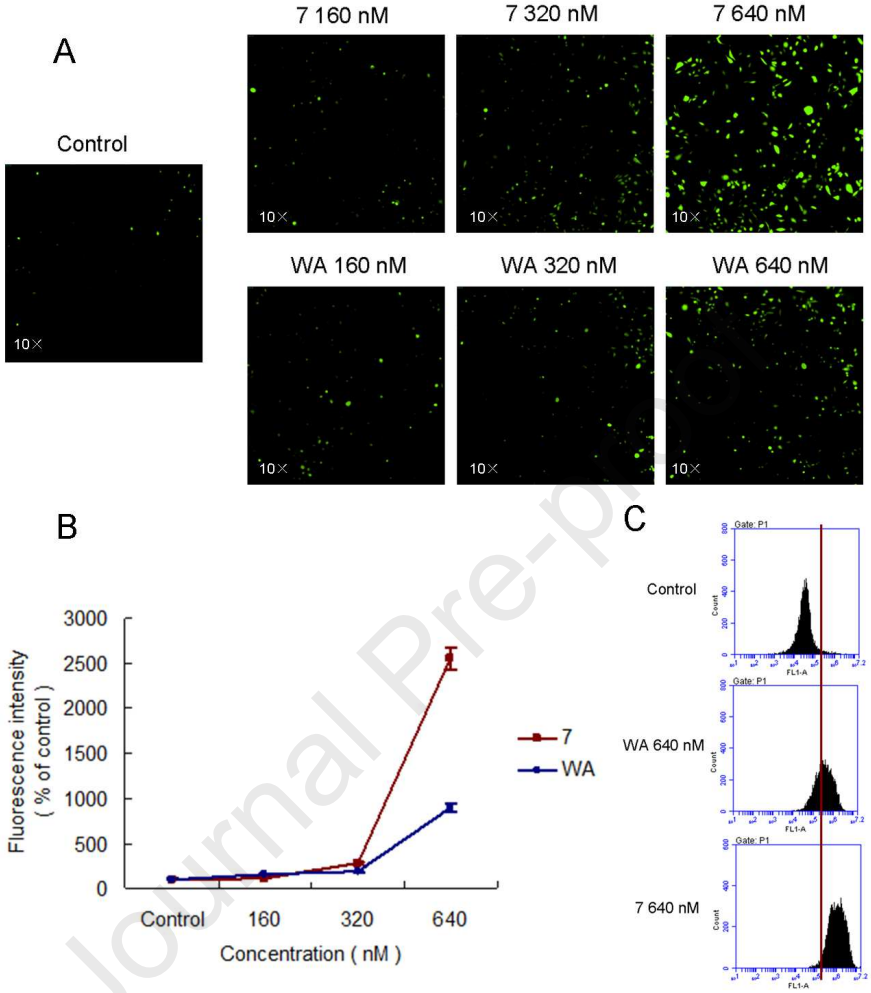

Fig. 6. ROS activity. 10000/well A549 cells treated or not treated (Ctrl) with different concentration of **7**, or **WA** (0, 160, 320, or 640 nM) for 3 h. (A) Fluorescence microscopic images of intracellular ROS production by DCFH-DA staining (green) in MDA-MB-231 cells (B) Quantitative analysis of ROS generation by the flow cytometry. (C) At a concentration of 640 nM, **7** showed improved ROS activity in comparison with control group and **WA**.

2.9. Molecular docking studies and binding pattern analysis

The structure of GLS1 has been determined, revealing the presence of four units in the asymmetric tetramer, which has been shown to be necessary for the catalytic activity of GLS1

[51]. In the crystal structure of GLS1, there were two main different binding pockets, a substrate binding pocket and an allosteric binding pocket for ligand to occupy inhibiting the enzyme activity of GLS1.

In order to investigate the possible binding pattern of compound **7** with GLS1, the docking study was conducted based on the GLS1 crystal structure (PDB code 3UO9). According to binding model, **7** was found to interact with a different reacting site of the allosteric pocket in GLS1 (**Fig. 7A** and **B**). The acetoxyl in inhibitor **7** could form hydrogen bonding contact with the protein backbone amide groups of LYS-320. The two carbonyl groups of the linker made hydrogen bonds with ARG-317 and another LYS-320. These H-bond interactions allowed this linker to protrude into the narrow active-site channel formed by the tetramer of GLS1, thus orientating the 4-morpholinoaniline moiety into another binding site region. Then the morpholine ring of **7** linked to phenyl ring bound to the inner pocket and made a hydrogen bond with the residue of LYS-320. The phenyl ring formed strong π- π stacked interactions with the residues of ARG-317. All interactions helped stabilize the conformation and combination of the ligand lying in the new site of the allosteric pocket of GLS1. Furthermore, different from the docking result of **WA** which only made hydrogen bonds with LYS-320 (**Fig. 7C** and **D**), **7** had a stronger binding capacity. Moreover, **7** took a different binding mode from that of BPTES and its analogs of which the thiadiazole group and the aliphatic linker occupy the allosteric pocket by forming hydrogen bonds with Lys320, Leu323 and Leu321 [40]. Collectively, **7** exploited the GLS1 allosteric binding site via three distinct parts of the molecule including **WA**, linker, and the substituent.

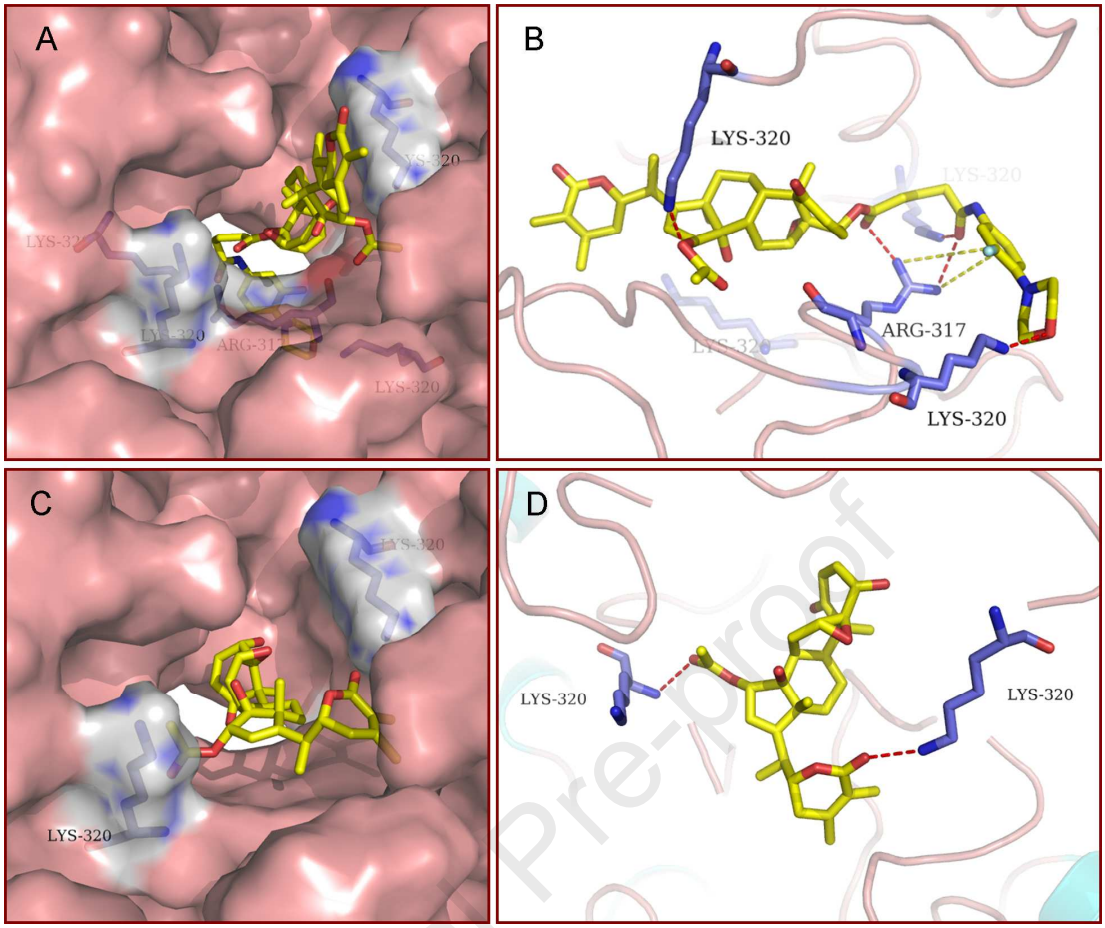

Fig. 6. Docking studies results of **7** in GLS1 (PDB code 3UO9). (A) **7** shown with the protein surface representation of GLS1; (B) Key interactions of **7** with GLS1; (C) **WA** shown with the protein surface representation of GLS1; (D) Key interactions of **WA** with GLS1. **7** and **WA** are rendered as a stick and colored by atom type, with yellow carbons, blue nitrogens, and red oxygens. The key residue atoms in GLS1 which interact with compound **7** are shown as sticks and colored by atom type, with light blue carbon, red oxygen, and blue nitrogen, and their surface is colored according to the coulombic potential. The yellow dashed lines represent the π- π interactions. The red dashed lines represent the hydrogen bonds.

*2.10. Compound **7** suppressed tumor growth in vivo*

To investigate the antitumor activity of compound **7** in vivo, we established a xenograft model by subcutaneously injecting MDA-MB-231 cells in nude mice. After four weeks of treatment by **7** (i.p., 25 and 50 mg/kg per 3 days) and BPTES (i.p., 25 mg/kg per 3 days), the mice were euthanized, and their organs were harvested for histopathologic analysis. As

shown in **Fig. 8A**, the growths of tumors were effectively inhibited in the **7**-treated groups compared with the vehicle group. Tumor volume and tumor weight were observably reduced after treatment with **7** (**Fig. 8B and C**). Moreover, compound **7** had no significant effect on the body weight of mice or obvious signs of adverse effects during the experimental treatment period (**Fig. 8D**). To investigate the effect of compound **7** on organ damage, the H&E staining of heart, liver, spleen, lung, and kidney tissues were analyzed. The histopathological morphology changes of organs were not detected in compound **7**-treated tumor-bearing mouse group, which showed that there was no obvious toxicity under the current treatment paradigm (**Fig. S31**). These results clearly indicated that compound **7** effectively inhibited the tumor proliferation in a preclinical mouse model without causing apparent toxicity.

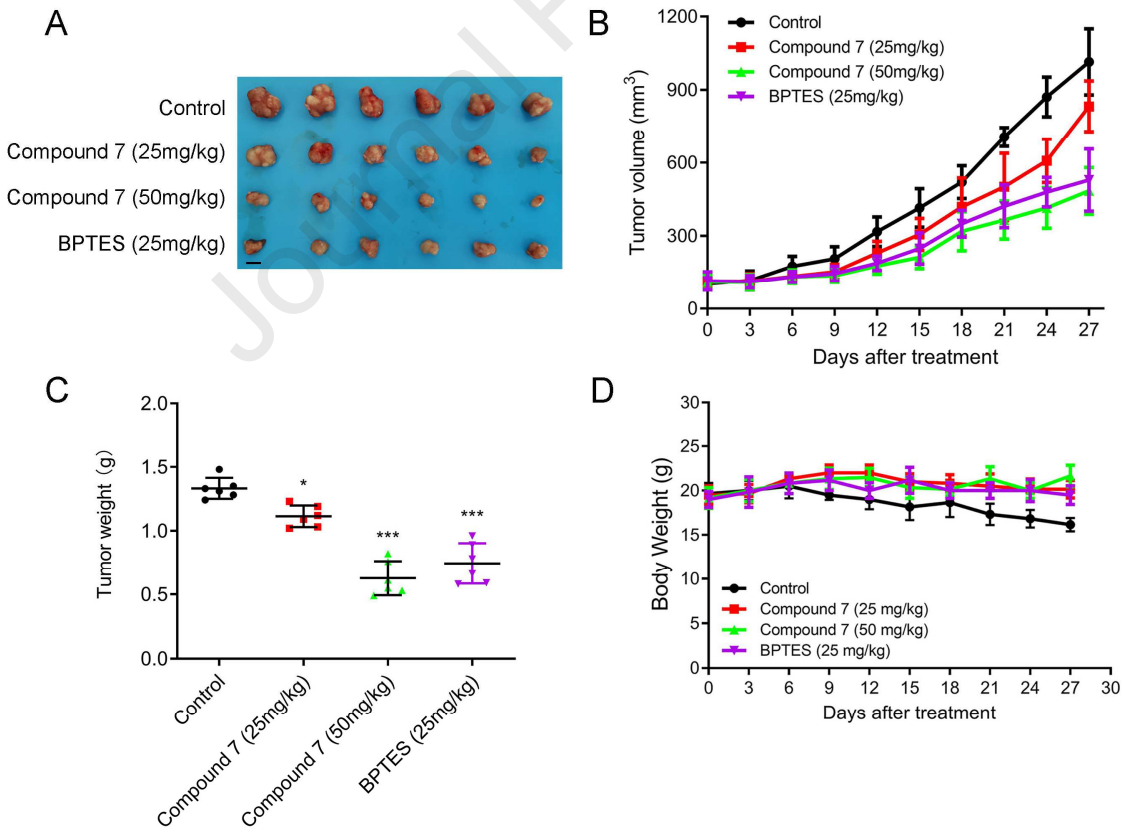

Fig. 7. Compound **7** inhibited TNBC growth in vivo. (A) Images of MDA-MB-231 tumor-bearing mice

after treated with **7** or BPTES. Changes of tumor volume (B), tumor weight (C), and body weight (D) were shown. Data represent the means ± SD (n = 6), **P* < 0.05, ****P* < 0.001, compared with control group. Scale bar = 5 mm.

3. Conclusion

A series of **WA** derivatives in which a 4-hydroxyl group was modified with different types of substituents derived from BPTES via different linkers were designed, synthesized, and evaluated as potential GLS1 inhibitors. These **WA**-based core compounds showed strong antiproliferative activity against MDA-MB-231 cells bearing overexpressed GLS1. Among them, **7** exhibited stronger inhibition against GLS1 compared with **WA** and BPTES in enzyme assay. Compound **7** could diminish cellular glutamate levels by blocking glutaminolysis pathway, further triggering the generation of reactive oxygen species, thus inducing caspase-dependent apoptosis. According to binding model, **7** exhibited a different binding pattern from **WA** and BPTES, which exploited the GLS1 allosteric binding site via three characteristic parts of the molecule including **WA**, linker, and the substituent. Moreover, compound **7** effectively inhibited the MDA-MB-231 xenograft tumor growth without apparent toxicity. As a result, **7** showed promising application as a GLS1 inhibitor from a natural product for the treatment of TNBC that deserves further development.

4. Experimental

4.1. Chemistry

4.1.1. General methods

All solvents were reagent grade or HPLC grade. Unless otherwise specified, all materials were obtained from commercial suppliers (Sigma-Aldrich, Ark-Pharm, TCI, Aladdin or Energy Chemical) and used as supplied without further purification. **WA**, used as starting

material, was isolated from *Physalis angulata var. villosa* by our group, and its structure was identified by ESIMS and NMR. All the reactions were monitored by TLC analysis. Analytical TLC was carried out on silica gel plates HSGF254. Chromatographic purification was conducted on commercial silica gel column (200-300 meshes, Qingdao Haiyang Chemical Co., Ltd., China). Preparative HPLC purification was performed on Shimadzu apparatus with a 1200 series multi-wavelength detector using a Shim-pack RP-C18 column (20 × 200 mm, i.d.) at a flow rate of 10 mL/min. All final compounds have purity ≥ 95% as determined by an Agilent1260 instrument equipped with multiple wavelength diode array detector. ^{1}H (500 MHz) and ^{13}C (126 MHz) nuclear magnetic resonance (NMR) spectra were measured on a Bruker ACF-500 NMR instrument (Bruker, Karlsruhe, Germany) at ambient temperature using TMS as the internal standard. Solutions were prepared in $CDCl_3$ with chemical shifts (δ) which are given in ppm referenced to deuterated solvent as an internal standard. High-resolution ESI mass spectrometry (HRMS) data were acquired on an Agilent 6520B Q-TOF mass instrument (Agilent, America).

*4.1.2. Procedure for synthesis of intermediate **a***

The preparation of **a** was performed following the route illustrated in **Schemes 1** and **2**. **WA** (1 eq., 20 mg, 0.038 mmol) was dissolved in pre-dried DCM (0.5 mL). Then TEA (0.5 mL) and glutaric anhydride (1.5 eq., 6.5 mg, 0.057 mmol) was added at room temperature. The reaction mixture was stirred for 72 h in refluxing. The mixture was washed with water (1 mL × 3) and brine (1 mL × 3), respectively. The organic layers were dried over Na_2SO_4 and concentrated in vacuo. The residue was purified by silica gel column chromatography (hexanes/EtOAc = 1/30) to get the desired pure product **a**.

4.1.2.1. (20S, 22R)-15α-acetoxy-5β,6β-epoxy-14β-dihydroxy-1-oxowitha-2,16,24-trienolide-4β-yl

*hemiglutarate (**a**).* Pale yellow amorphous powder. Yield: 21.9 mg (90.2%). ^{1}H NMR (500 MHz, $CDCl_3$), δ 7.05 (1H, dd, *J* = 9.8, 6.0 Hz, H-3), 6.24 (1H, d, *J* = 9.8 Hz, H-2), 5.68 (1H, d, *J* = 2.5 Hz, H-16), 5.22 (1H, d, *J* = 2.6 Hz, H-15), 4.75 (1H , d, *J* = 6.0 Hz, H-4), 4.23 (1H, ddd, *J* = 12.3, 6.6, 3.4 Hz, H-22), 3.35 (1H, s, H-6), 1.94 (3H, s, -COC$\underline{H}_3$), 1.93 (3H, s, Me-28), 1.90 (3H, s, Me-27), 1.39 (3H, s, Me-19), 1.11 (3H, d, *J* = 7.0 Hz, Me-21), 1.08 (3H, s, Me-18). ^{13}C NMR (126 MHz, $CDCl_3$), δ 201.5 (C-1), 176.4 (-COOH), 172.1 (-COO-), 169.7 (-COCH3), 166.3 (C-26), 162.5 (C-17), 148.6 (C-24), 140.5 (C-3), 133.3 (C-2), 122.3 (C-25), 121.1 (C-16), 83.7 (C-15), 81.6 (C-14), 79.4 (C-22), 72.0 (C-4), 61.3 (C-5), 60.4 (C-6), 52.2 (C-13), 48.1 (C-10), 39.6 (C-9), 37.4 (C-12), 35.5 (C-20), 34.6 (C-8), 33.1 (C-23), 33.1 (-OCO-$\underline{C}H_2$-CH_2-CH_2-COOH), 32.6 (-OCO-CH_2-CH_2-$\underline{C}H_2$-COOH), 24.6 (C-7), 21.5 (C-11), 21.1 (-CO$\underline{C}H_3$), 20.6 (C-28), 19.9 (-OCO-CH_2-$\underline{C}H_2$-CH_2-COOH), 17.7 (C-21), 16.0 (C-19), 15.8 (C-18), 12.6 (C-27). HRMS m/z calculated for $C_{35}H_{44}O_{11}$, 640.2884; found $[M + H]^+$, 641.2856.

*4.1.3. Procedure for synthesis of intermediate **b***

The preparation of **b** was performed following the route illustrated in **Schemes 1** and **2**. **WA** (1 eq., 20 mg, 0.038 mmol) was dissolved in pre-dried DCM (0.5 mL). Then TEA (0.5 mL) and succinic anhydride (1.5 eq., 5.7 mg, 0.057 mmol) was added at room temperature. The reaction mixture was stirred for 50 h in refluxing. The mixture was washed with water (1 mL × 3) and brine (1 mL × 3), respectively. The organic layers were dried over Na_2SO_4 and concentrated in vacuo. The residue was purified by silica gel column chromatography (EtOAc) to get the desired pure product **b**.

*4.1.3.1. (20S, 22R)-15α-acetoxy-5β,6β-epoxy-14β-dihydroxy-1-oxowitha-2,16,24-trienolide-4β-yl hemisuccinate (**b**).* Pale yellow amorphous powder. Yield: 23.3 mg (98.0%). ^{1}H NMR (500

MHz, $CDCl_3$), δ 7.05 (1H, dd, J = 9.7, 6.1 Hz, H-3), 6.19 (1H, d, J = 9.7 Hz, H-2), 5.66 (1H, d, J = 2.3 Hz, H-16), 5.20 (1H, d, J = 2.5 Hz, H-15), 4.72 (1H , d, J = 6.1 Hz, H-4), 4.23 (1H, ddd, J = 10.7, 6.7, 3.4 Hz, H-22), 3.31 (1H, s, H-6), 1.92 (3H, s, -COC$\underline{H}_3$), 1.92 (3H, s, Me-28), 1.84 (3H, s, Me-27), 1.39 (3H, s, Me-19), 1.10 (3H, d, J = 7.0 Hz, Me-21), 1.07 (3H, s, Me-18). ^{13}C NMR (126 MHz, $CDCl_3$), δ 201.6 (C-1), 177.7 (-COOH), 172.9 (-COO-), 169.7 (-COCH3), 166.4 (C-26), 162.3 (C-17), 148.8 (C-24), 141.0 (C-3), 133.0 (C-2), 122.2 (C-25), 122.0 (C-16), 83.8 (C-15), 81.6 (C-14), 79.3 (C-22), 71.6 (C-4), 61.1 (C-5), 60.4 (C-6), 52.2 (C-13), 48.0 (C-10), 39.7 (C-9), 37.5 (C-12), 35.5 (C-20), 34.7 (C-8), 33.1 (C-23), 31.7 (-OCO-$\underline{C}H_2$-CH_2-COOH), 30.8 (-OCO-CH_2-$\underline{C}H_2$-COOH), 24.6 (C-7), 21.4 (C-11), 21.1 (-CO$\underline{C}H_3$), 20.5 (C-28), 17.7 (C-21), 16.0 (C-19), 15.8 (C-18), 12.5 (C-27). HRMS m/z calculated for $C_{34}H_{42}O_{11}$, 626.2727; found $[M + H]^+$, 627.2788.

*4.1.4. Procedure for synthesis of intermediate **c***

The preparation of **c** was performed following the route illustrated in **Schemes 1** and **2**. **WA** (1 eq., 20 mg, 0.038 mmol) was dissolved in pre-dried DCM (0.5 mL). Then TEA (0.5 mL) and maleic anhydride (1.5 eq., 5.6 mg, 0.057 mmol) was added at room temperature. The reaction mixture was stirred for 40 h in refluxing. The mixture was washed with water (1 mL × 3) and brine (1 mL × 3), respectively. The organic layers were dried over Na_2SO_4 and concentrated in vacuo. The residue was purified by silica gel column chromatography (hexanes/EtOAc = 1/20) to get the desired pure product **c**.

*4.1.4.1. (20S, 22R)-15α-acetoxy-5β,6β-epoxy-14β-dihydroxy-1-oxowitha-2,16,24-trienolide-4β-yl hemimaleate (**c**).* Pale yellow amorphous powder. Yield: 22.9 mg (96.5%). ^{1}H NMR (500 MHz, $CDCl_3$), δ 7.06 (1H, dd, J = 9.8, 6.0 Hz, H-3), 6.57 (1H, d, J = 12.0 Hz, -$\underline{C}$=C-), 6.20 (1H, d, J = 9.8 Hz, H-2), 5.69 (1H, d, J = 12.0 Hz, -C=$\underline{C}$-), 5.66 (1H, d, J = 2.2 Hz, H-16),

5.21 (1H, d, *J* = 2.5 Hz, H-15), 4.79 (1H , d, *J* = 6.0 Hz, H-4), 4.24 (1H, ddd, *J* = 10.3, 6.4, 3.4 Hz, H-22), 3.32 (1H, s, H-6), 1.92 (3H, s, -COC<u>H</u>$_3$), 1.92 (3H, s, Me-28), 1.84 (3H, s, Me-27), 1.37 (3H, s, Me-19), 1.10 (3H, d, *J* = 7.0 Hz, Me-21), 1.06 (3H, s, Me-18). ^{13}C NMR (126 MHz, $CDCl_3$), *δ* 201.7 (C-1), 172.3 (-COOH), 169.7 (-COCH3), 166.4 (C-26), 165.1 (-COO-), 162.3 (C-17), 148.8 (C-24), 143.8 (-<u>C</u>H=CH-), 141.1 (C-3), 133.1 (C-2), 122.2 (C-25), 121.0 (C-16), 116.9 (-CH=<u>C</u>H-), 83.8 (C-15), 81.6 (C-14), 79.3 (C-22), 71.4 (C-4), 61.1 (C-5), 60.5 (C-6), 52.2 (C-13), 48.0 (C-10), 39.8 (C-9), 37.5 (C-12), 35.5 (C-20), 34.7 (C-8), 33.0 (C-23), 24.6 (C-7), 21.5 (C-11), 21.1 (-CO<u>C</u>H$_3$), 20.6 (C-28), 17.7 (C-21), 16.0 (C-19), 15.8 (C-18), 12.5 (C-27). HRMS m/z calculated for $C_{34}H_{40}O_{11}$, 624.2571; found $[M + H]^+$, 625.2605.

4.1.5. Procedure for synthesis of intermediate ***d***

To a mixture of morpholine (2 eq., 2.4 g, 27.1 mmol) and KH_2PO_4 (2 eq., 4.7 g, 27.1 mmol) in DMSO (24 mL) was added 3, 4 - difluoronitrobenzene (1 eq., 2.2 g, 13.6 mmol), and the resulting mixture was stirred at 60 ºC for 24 h. The resulting solution was added to cool water, and extracted with ethyl acetate (50 mL × 3). The organic layer was dried over Na_2SO_4, filtered and concentrated under vacuum to give a yellow solid (yield: 2.9 g, 94.2%). The solid (2.9 g, 12.8 mmol) was dissolved in ethyl acetate (60 mL), and 10% Pd-C (10%, 0.3 g) was added. The resulting mixture was stirred under H_2 for 6 h. The mixture was filtered and the filtrate was concentrated under vacuum to give **d** [52].

*4.1.5.1. 3-fluoro-4-morpholinoaniline (**d**)*. Pale brown solid. Yield: 2.3 g (87.6%). ^{1}H NMR (500 MHz, $CDCl_3$), The hydrogen signals of the phenyl ring [*δ* 6.78 (1H, t, *J* = 8.8), 6.39 (2H, m)], 3.83 (4H, t, *J* = 4.2 Hz, -(C<u>H</u>$_2$-)$_2$O), 2.95 (4H, t, *J* = 3.9 Hz, -N(-C<u>H</u>$_2$-)$_2$). ^{13}C NMR (126 MHz, $CDCl_3$), The carbon signals of the phenyl ring [*δ* 157.8, 143.0, 131.8, 120.4, 110.7, 104.0], 67.2 (-(<u>C</u>H$_2$-)$_2$O), 67.2 (-(<u>C</u>H$_2$-)$_2$O), 51.8 (-N(-<u>C</u>H$_2$-)$_2$), 51.8 (-N(-<u>C</u>H$_2$-)$_2$).

*4.1.6. General procedure for synthesis of compounds **1-21***

EDCI·HCl (2.2 eq.), HOBt·H_2O (1.5 eq.), and pyridine (3.0 eq.) were added to a solution of Acid (the intermediates a, b, or c; 1.0 eq.) in DMF at room temperature under N_2 atmosphere. After 30 min, a solution of R_2-H (Scheme 1; 1.2 eq.) in DMF was added dropwise. The mixture was then stirred for 15 h at room temperature and, upon completion of the reaction, water was added and extracted with EtOAc. The organic layers were then washed with brine, dried over Na_2SO_4, filtered and concentrated in vacuo. The residue was purified via preparative HPLC using acetonitrile/water (1/1) as the solvent system to obtain the target compounds.

*4.1.6.1. (20S, 22R)-15α-acetoxy-5β,6β-epoxy-14β-dihydroxy-1-oxowitha-2,16,24-trienolide-4β-yl 5-((1,3,4-thiadiazol-2-yl)amino)-5-oxopentanoate (**1**).* Pale yellow amorphous powder. Yield: 15.4 mg (56.2%). ^{1}H NMR (500 MHz, $CDCl_3$), δ 8.80 (1H, s, -SC<u>H</u>=N-), 6.98 (1H, dd, *J* = 9.9, 5.8 Hz, H-3), 6.25 (1H, d, *J* = 9.9 Hz, H-2), 5.69 (1H, d, *J* = 2.6 Hz, H-16), 5.23 (1H, d, *J* = 2.7 Hz, H-15), 4.90 (1H , d, *J* = 5.8 Hz, H-4), 4.27 (1H, ddd, *J* = 12.7, 6.0, 3.5 Hz, H-22), 3.45 (1H, s, H-6), 1.95 (3H, s, -COC<u>H</u>$_3$), 1.93 (3H, s, Me-28), 1.86 (3H, s, Me-27), 1.38 (3H, s, Me-19), 1.13 (3H, d, *J* = 7.0 Hz, Me-21), 1.11 (3H, s, Me-18). ^{13}C NMR (126 MHz, $CDCl_3$), δ 201.7 (C-1), 171.9 (-<u>C</u>ONH-), 170.8 (-<u>C</u>OO-), 169.7 (-<u>C</u>OCH$_3$), 166.4 (C-26), 161.9 (C-17), 159.6 (-S<u>C</u>N-NH-), 148.8 (C-24), 147.7 (-S<u>C</u>HN-), 140.2 (C-3), 133.2 (C-2), 122.3 (C-25), 121.4 (C-16), 83.8 (C-15), 81.6 (C-14), 79.0 (C-22), 71.4 (C-4), 62.8 (C-5), 61.2 (C-6), 52.3 (C-13), 48.1 (C-10), 39.8 (C-9), 37.3 (C-12), 35.4 (C-20), 35.1 (C-8), 34.9 (C-23), 33.6 (-NHCO<u>C</u>H$_2$-), 32.6 (-OCO<u>C</u>H$_2$-), 24.7 (C-7), 21.6 (C-11), 21.5 (-CO<u>C</u>H$_3$), 21.1 (-CH$_2$<u>C</u>H$_2$CH$_2$-), 20.6 (C-28), 17.4 (C-21), 16.5 (C-19), 16.0 (C-18), 12.6 (C-27). HRMS m/z calculated for $C_{37}H_{45}N_3O_{10}S$, 723.2826; found $[M + H]^+$, 724.2857.

4.1.6.2. *(20S, 22R)-15α-acetoxy-5β,6β-epoxy-14β-dihydroxy-1-oxowitha-2,16,24-trienolide-4β-yl 5-oxo-5-(thiazol-2-ylamino)pentanoate (**2**).* Pale yellow amorphous powder. Yield: 13.6 mg (49.5%). ^{1}H NMR (500 MHz, $CDCl_3$), δ 7.43 (1H, d, *J* = 7.2 Hz, =NC<u>H</u>=CHS-),7.00 (1H, d, *J*=6.0 Hz, -SC<u>H</u>=CHN=), 6.96 (1H, dd, *J* = 9.9, 5.8 Hz, H-3), 6.25 (1H, d, *J*=9.9 Hz, H-2), 5.70 (1H, d, *J*=2.6 Hz, H-16), 5.22 (1H, d, *J*=2.7 Hz, H-15), 4.94 (1H , d, *J* =5.8 Hz, H-4), 4.26 (1H, ddd, *J*=12.7, 6.1, 3.5 Hz, H-22), 3.46 (1H, s, H-6), 1.95 (3H, s, -COC<u>H</u>$_3$), 1.93 (3H, s, Me-28), 1.86 (3H, s, Me-27), 1.38 (3H, s, Me-19), 1.13 (3H, d, *J* = 7.0 Hz, Me-21), 1.08 (3H, s, Me-18). ^{13}C NMR (126 MHz, $CDCl_3$), δ 201.8 (C-1), 172.1 (-<u>C</u>ONH-), 170.4 (-<u>C</u>OO-), 169.8 (-<u>C</u>OCH$_3$), 166.4 (C-26), 162.0 (C-17), 159.2 (-N=<u>C</u>-S-), 148.8 (C-24), 140.2 (C-3), 136.1 (=N<u>C</u>H=CHS-), 133.0 (C-2), 122.3 (C-25), 121.3 (C-16), 113.7 (-S<u>C</u>H=CHN=), 83.8 (C-15), 81.5 (C-14), 79.1 (C-22), 71.0 (C-4), 63.0 (C-5), 61.3 (C-6), 52.2 (C-13), 48.0 (C-10), 39.7 (C-9), 37.3 (C-12), 35.3 (C-20), 35.0 (C-8), 34.9 (C-23), 33.6 (-NHCO<u>C</u>H$_2$-), 32.6 (-OCO<u>C</u>H$_2$-), 24.7 (C-7), 21.8 (C-11), 21.5 (-CO<u>C</u>H$_3$), 21.0 (C-28), 20.6 (-CH$_2$<u>C</u>H$_2$CH$_2$-), 17.4 (C-21), 16.7 (C-19), 16.1 (C-18), 12.6 (C-27). HRMS m/z calculated for $C_{38}H_{46}N_2O_{10}S$, 722.2873; found $[M + H]^+$, 723.2906.

4.1.6.3. *(20S, 22R)-15α-acetoxy-5β,6β-epoxy-14β-dihydroxy-1-oxowitha-2,16,24-trienolide-4β-yl 5-(benzo[d]thiazol-2-ylamino)-5-oxopentanoate (**3**).* Pale yellow amorphous powder. Yield: 20.2 mg (68.7%). ^{1}H NMR (600 MHz, $CDCl_3$), The hydrogen signals of the benzene ring [δ 7.82 (1H, d, *J* = 7.8 Hz), 7.76 (1H, d, *J* = 8.1 Hz), 7.42 (1H, t, *J* = 7.6 Hz), 7.32 (1H, t, *J* = 7.6 Hz)], 6.99 (1H, dd, *J* = 9.9, 5.8 Hz, H-3), 6.26 (1H, d, *J*=9.9 Hz, H-2), 5.71 (1H, d, *J*=2.5 Hz, H-16), 5.24 (1H, d, *J*=2.6 Hz, H-15), 4.89 (1H , d, *J* = 5.8 Hz, H-4), 4.25 (1H, ddd, *J*=12.6, 6.1, 3.4 Hz, H-22), 3.46 (1H, s, H-6), 1.95 (3H, s, -COC<u>H</u>$_3$), 1.94 (3H, s, Me-28), 1.87 (3H, s, Me-27), 1.38 (3H, s, Me-19), 1.13 (3H, d, *J* = 7.0 Hz, Me-21), 1.04 (3H, s, Me-18). ^{13}C NMR

(151 MHz, $CDCl_3$), δ 201.8 (C-1), 172.1 (-CONH-), 170.9 (-COO-), 169.7 (-$COCH_3$), 166.4 (C-26), 162.1 (C-17), 158.6 (-SC=N-), 148.7 (C-24), 140.3 (C-3), 133.1 (C-2), 122.3 (C-25), 121.3 (C-16), The carbon signals of the benzene ring [147.4, 131.8, 126.5, 124.3, 121.7, 120.7], 83.7 (C-15), 81.5 (C-14), 79.1 (C-22), 71.4 (C-4), 62.5 (C-5), 61.1 (C-6), 52.2 (C-13), 48.0 (C-10), 39.6 (C-9), 37.3 (C-12), 35.3 (C-20), 35.1 (-NHCOCH_2-), 34.9 (-OCOCH_2-), 33.4 (C-8), 32.7 (C-23), 24.6 (C-7), 21.5 (C-11), 21.5 (-$CH_2CH_2CH_2$-), 20.8 (-COCH_3), 20.6 (C-28), 17.4 (C-21), 16.5 (C-19), 16.0 (C-18), 12.6 (C-27). HRMS m/z calculated for $C_{42}H_{48}N_2O_{10}S$, 772.3030; found $[M + H]^+$, 773. 3102.

*4.1.6.4. (20S, 22R)-15α-acetoxy-5β,6β-epoxy-14β-dihydroxy-1-oxowitha-2,16,24-trienolide-4β-yl 5-((4-fluorophenyl)amino)-5-oxopentanoate (**4**).* Pale yellow amorphous powder. Yield: 12.3 mg (44.1%). ^{1}H NMR (500 MHz, $CDCl_3$), *δ* 7.84 (1H, s, -CONH-), The hydrogen signals of the phenyl ring [7.55 (2H, dd, *J* = 9.0, 4.8 Hz), 7.00 (2H, t, *J* = 8.7 Hz)], 7.07 (1H, dd, *J* = 9.8, 6.0 Hz, H-3), 6.26 (1H, d, *J* = 9.8 Hz, H-2), 5.68 (1H, d, *J* = 2.6 Hz, H-16), 5.23 (1H, d, *J* = 2.7 Hz, H-15), 4.77 (1H , d, *J* = 6.0 Hz, H-4), 4.23 (1H, ddd, *J* = 12.3, 7.1, 3.5 Hz, H-22), 3.41 (1H, s, H-6), 1.94 (3H, s, -COCH_3), 1.93 (3H, s, Me-28), 1.85 (3H, s, Me-27), 1.33 (3H, s, Me-19), 1.11 (3H, d, *J* = 7.0 Hz, Me-21), 1.06 (3H, s, Me-18). ^{13}C NMR (126 MHz, $CDCl_3$), *δ* 202.0 (C-1), 172.3 (-CONH-), 170.4 (-COO-), 169.7 (-$COCH_3$), 166.2 (C-26), 162.6 (C-17), 148.6 (C-24), 140.6 (C-3), 133.3 (C-2), 122.3 (C-25), 120.9 (C-16), The carbon signals of the phenyl ring [158.4, 134.4, 121.6, 121.6, 115.8, 115.6], 83.7 (C-15), 81.5 (C-14), 79.5 (C-22), 72.0 (C-4), 61.8 (C-5), 60.7 (C-6), 52.1 (C-13), 48.2 (C-10), 39.6 (C-9), 37.4 (C-12), 36.2 (-NHCOCH_2-), 35.5 (C-20), 34.4 (C-8), 33.5 (C-23), 33.3 (-OCOCH_2-), 24.6 (C-7), 21.5 (C-11), 21.4 (-COCH_3), 21.1 (-CH_2-CH_2-CH_2-), 20.6 (C-28), 17.9 (C-21), 16.0 (C-19), 15.9 (C-18), 12.6 (C-27). HRMS m/z calculated for $C_{41}H_{48}FNO_{10}$, 733.3262; found $[M + Na]^+$, 756.3125.

4.1.6.5. *(20S, 22R)-15α-acetoxy-5β,6β-epoxy-14β-dihydroxy-1-oxowitha-2,16,24-trienolide-4β-yl 5-((4-(dimethylamino)phenyl)amino)-5-oxopentanoate (**5**).* Yellow amorphous powder. Yield: 12.2 mg (42.5%). ^{1}H NMR (500 MHz, $CDCl_3$), The hydrogen signals of the phenyl ring [δ 7.41 (2H, d, *J* = 8.9 Hz), 6.71 (2H, d, *J* = 7.8 Hz)], δ 7.05 (1H, dd, *J* = 9.8, 6.0 Hz, H-3), 6.25 (1H, d, *J* = 9.8 Hz, H-2), 5.68 (1H, d, *J* = 2.1 Hz, H-16), 5.22 (1H, d, *J* = 2.6 Hz, H-15), 4.78 (1H , d, *J* = 5.9 Hz, H-4), 4.23 (1H, ddd, *J* = 12.4, 7.0, 3.5 Hz, H-22), 3.47 (1H, s, H-6), 2.90 (6H, s, -N(-C<u>H</u>$_3$)), 1.94 (3H, s, -COC<u>H</u>$_3$), 1.93 (3H, s, Me-28), 1.85 (3H, s, Me-27), 1.35 (3H, s, Me-19), 1.11 (3H, d, *J* = 7.0 Hz, Me-21), 1.06 (3H, s, Me-18). ^{13}C NMR (126 MHz, $CDCl_3$), δ 201.9 (C-1), 172.4 (-<u>C</u>ONH-), 170.1 (-<u>C</u>OO-), 169.7 (-<u>C</u>OCH$_3$), 166.3 (C-26), 162.5 (C-17), 148.6 (C-24), 140.6 (C-3), 133.2 (C-2), 122.3 (C-25), 120.9 (C-16), The carbon signals of the phenyl ring [162.4, 128.3, 121.7, 121.7, 113.4, 113.4], 83.7 (C-15), 81.5 (C-14), 79.4 (C-22), 71.8 (C-4), 61.8 (C-5), 60.7 (C-6), 52.3 (C-13), 48.1 (C-10), 41.2 (-N(-<u>C</u>H$_3$)$_2$), 41.2 (-N(-<u>C</u>H$_3$)$_2$), 39.6 (C-9), 37.4 (C-12), 36.2 (-NHCO<u>C</u>H$_2$-), 35.5 (C-20), 34.6 (C-8), 33.5 (C-23), 33.2 (-OCO<u>C</u>H$_2$-), 24.6 (C-7), 21.5 (-(-<u>C</u>H$_2$)-), 21.2 (C-11), 20.6 (-CO<u>C</u>H$_3$), 19.5 (C-28), 17.8 (C-21), 16.0 (C-19), 16.0 (C-18), 12.6 (C-27). HRMS m/z calculated for $C_{43}H_{54}N_2O_{10}$, 758.3778; found $[M + H]^+$, 759.3809.

4.1.6.6. *(20S, 22R)-15α-acetoxy-5β,6β-epoxy-14β-dihydroxy-1-oxowitha-2,16,24-trienolide-4β-yl 5-((4-methoxyphenyl)amino)-5-oxopentanoate (**6**).* Pale yellow amorphous powder. Yield: 16.5 mg (58.2%). ^{1}H NMR (500 MHz, $CDCl_3$), δ 7.70 (1H, s, -CON<u>H</u>-), The hydrogen signals of the phenyl ring [7.47 (2H, d, *J* = 9.0 Hz), 6.84 (2H, d, *J* = 9.0 Hz)], 7.06 (1H, dd, *J* = 9.8, 6.0 Hz, H-3), 6.25 (1H, d, *J* = 9.8 Hz, H-2), 5.68 (1H, d, *J* = 2.6 Hz, H-16), 5.22 (1H, d, *J* = 2.7 Hz, H-15), 4.78 (1H , d, *J* = 5.9 Hz, H-4), 4.22 (1H, ddd, *J* = 12.3, 6.9, 3.5 Hz, H-22), 3.40 (1H, s, H-6), 1.94 (3H, s, -COC<u>H</u>$_3$), 1.92 (3H, s, Me-28), 1.85 (3H, s, Me-27), 1.34 (3H,

s, Me-19), 1.11 (3H, d, *J* = 7.0 Hz, Me-21), 1.06 (3H, s, Me-18). ^{13}C NMR (126 MHz, $CDCl_3$), *δ* 201.9 (C-1), 172.3 (-CONH-), 170.2 (-COO-), 169.7 (-$COCH_3$), 166.2 (C-26), 162.6 (C-17), 148.6 (C-24), 140.6 (C-3), 133.2 (C-2), 122.3 (C-25), 120.9 (C-16), The carbon signals of the phenyl ring [156.4, 131.4, 122.1, 121.7, 121.6, 114.2], 83.7 (C-15), 81.5 (C-14), 79.5 (C-22), 71.9 (C-4), 61.8 (C-5), 60.7 (C-6), 55.6 (-OCH_3), 52.1 (C-13), 48.1 (C-10), 39.6 (C-9), 37.4 (C-12), 36.1 (-NHCOCH_2-), 35.5 (C-20), 34.5 (C-8), 33.5 (C-23), 33.2 (-OCOCH_2-), 24.6 (C-7), 21.5 (C-11), 21.4 (-COCH_3), 21.1 (-CH_2-CH_2-CH_2-), 20.6 (C-28), 17.8 (C-21), 16.0 (C-19), 15.9 (C-18), 12.6 (C-27). HRMS m/z calculated for $C_{42}H_{51}NO_{11}$, 745.3462; found $[M + H]^+$, 746.3485.

*4.1.6.7. (20S, 22R)-15α-acetoxy-5β,6β-epoxy-14β-dihydroxy-1-oxowitha-2,16,24-trienolide-4β-yl 5-((3-fluoro-4-morpholinophenyl)amino)-5-oxopentanoate (**7**).* Pale yellow amorphous powder. Yield: 17.1 mg (54.9%). ^{1}H NMR (500 MHz, $CDCl_3$), *δ* 7.78 (1H, s, -CONH-), The hydrogen signals of the phenyl ring [7.59 (1H, d, *J* = 14.4 Hz), 7.15 (1H, d, *J* = 7.6 Hz), 6.96 (1H, dd, *J* = 9.6, 5.9 Hz)], 7.07 (1H, dd, *J* = 9.8, 6.0 Hz, H-3), 6.27 (1H, d, *J* = 9.8 Hz, H-2), 5.70 (1H, d, *J* = 2.6 Hz, H-16), 5.25 (1H, d, *J* = 2.7 Hz, H-15), 4.79 (1H , d, *J* = 6.0 Hz, H-4), 4.22 (1H, ddd, *J* = 12.2, 7.4, 3.6 Hz, H-22), 3.87 (4H, t, *J* = 4.2 Hz, O(CH_2-)$_2$), 3.06 (4H, t, *J* = 3.9 Hz, -N(CH_2-)$_2$), 1.95 (3H, s, -COCH_3), 1.94 (3H, s, Me-28), 1.86 (3H, s, Me-27), 1.35 (3H, s, Me-19), 1.12 (3H, d, *J* = 7.0 Hz, Me-21), 1.07 (3H, s, Me-18). ^{13}C NMR (126 MHz, $CDCl_3$), *δ* 202.04 (C-1), 172.3 (-CONH-), 170.3 (-COO-), 169.7 (-$COCH_3$), 166.1 (C-26), 162.8 (C-17), 148.5 (C-24), 140.6 (C-3), 133.3 (C-2), 122.4 (C-25), 120.9 (C-16), The carbon signals of the phenyl ring [156.6, 154.6, 115.6, 115.6, 109.0, 108.8], 83.7 (C-15), 81.6 (C-14), 79.7 (C-22), 72.0 (C-4), 67.0 (C-5), 62.0 (C-6), 60.8 (-OCHCHN-), 60.5 (-OCHCHN-), 52.1 (C-13), 51.4 (-NCHCHO-), 51.4 (-NCHCHO-), 48.2 (C-10), 39.6 (C-9), 37.5 (C-12), 36.3 (C-20), 35.6 (C-8), 34.5 (C-23), 33.6 (-NHCOCH_2-), 33.4 (-OCOCH_2-), 24.6 (C-7), 21.5

(C-11), 21.5 (-CO<u>C</u>H$_3$), 21.2 (-CH$_2$<u>C</u>H$_2$CH$_2$-), 20.6 (C-28), 17.9 (C-21), 16.1 (C-19), 15.9 (C-18), 12.6 (C-27). HRMS m/z calculated for $C_{45}H_{55}FN_2O_{11}$, 818.3790; found $[M + H]^+$, 819.3858.

*4.1.6.8. (20S, 22R)-15α-acetoxy-5β,6β-epoxy-14β-dihydroxy-1-oxowitha-2,16,24-trienolide-4β-yl 4-((1,3,4-thiadiazol-2-yl)amino)-4-oxobutanoate (**8**).* Pale yellow amorphous powder. Yield: 14.8 mg (55.0%). ^{1}H NMR (600 MHz, $CDCl_3$), δ 8.82 (1H, s, -SC<u>H</u>=N-), 7.03 (1H, dd, *J* = 9.8, 6.0 Hz, H-3), 6.22 (1H, d, *J* = 9.8 Hz, H-2), 5.67 (1H, d, *J* = 2.4 Hz, H-16), 5.21 (1H, d, *J* = 2.6 Hz, H-15), 4.77 (1H , d, *J* = 6.0 Hz, H-4), 4.23 (1H, ddd, *J* = 12.5, 6.7, 3.5 Hz, H-22), 3.48 (1H, s, H-6), 1.92 (3H, s, -COC<u>H</u>$_3$), 1.92 (3H, s, Me-28), 1.85 (3H, s, Me-27), 1.34 (3H, s, Me-19), 1.11 (3H, d, *J* = 7.0 Hz, Me-21), 1.07 (3H, s, Me-18). ^{13}C NMR (151 MHz, $CDCl_3$), δ 201.3 (C-1), 171.4 (-<u>C</u>ONH-), 170.1 (-<u>C</u>OO-), 169.7 (-<u>C</u>OCH$_3$), 166.3 (C-26), 162.4 (C-17), 160.3 (-S<u>C</u>N-NH-), 148.7 (C-24), 147.7 (-S<u>C</u>HN-), 140.3 (C-3), 133.4 (C-2), 122.3 (C-25), 121.0 (C-16), 83.7 (C-15), 81.6 (C-14), 79.3 (C-22), 72.3 (C-4), 61.3 (C-5), 60.3 (C-6), 52.1 (C-13), 47.9 (C-10), 39.6 (C-9), 37.4 (C-12), 35.4 (C-20), 34.6 (C-8), 33.2 (C-23), 30.8 (-NHCO<u>C</u>H$_2$-), 28.9 (-OCO<u>C</u>H$_2$-), 24.5 (C-7), 21.5 (C-11), 21.1 (-CO<u>C</u>H$_3$), 20.6 (C-28), 17.7 (C-21), 16.0 (C-19), 15.8 (C-18), 12.6 (C-27). HRMS m/z calculated for $C_{36}H_{43}N_3O_{10}S$, 709.2669; found $[M + H]^+$, 710.2701.

*4.1.6.9. (20S, 22R)-15α-acetoxy-5β,6β-epoxy-14β-dihydroxy-1-oxowitha-2,16,24-trienolide-4β-yl 4-oxo-4-(thiazol-2-ylamino)butanoate (**9**).* Pale yellow amorphous powder. Yield: 12.4 mg (46.2%). ^{1}H NMR (500 MHz, $CDCl_3$), δ 7.48 (1H, d, *J* = 7.2 Hz, =NC<u>H</u>=CHS-), 7.02 (1H, m, H-3), 7.01 (1H, d, *J*=6.0 Hz, -SC<u>H</u>=CHN=), 6.24 (1H, d, *J*=9.8 Hz, H-2), 5.68 (1H, d, *J*=2.1 Hz, H-16), 5.21 (1H, d, *J*=2.7 Hz, H-15), 4.89 (1H , d, *J* = 6.0 Hz, H-4), 4.23 (1H, ddd,

J=12.3, 6.8, 3.4 Hz, H-22), 3.41 (1H, s, H-6), 1.95 (3H, s, -COC<u>H</u>$_3$), 1.93 (3H, s, Me-28), 1.86 (3H, s, Me-27), 1.41 (3H, s, Me-19), 1.11 (3H, d, *J* = 7.0 Hz, Me-21), 1.08 (3H, s, Me-18). ^{13}C NMR (126 MHz, $CDCl_3$), δ 201.2 (C-1), 171.4 (-<u>C</u>ONH-), 170.1 (-<u>C</u>OO-), 169.7 (-<u>C</u>OCH$_3$), 166.4 (C-26), 162.4 (C-17), 159.8 (-N=<u>C</u>-S-), 148.6 (C-24), 140.1 (C-3), 134.7 (=N<u>C</u>H=CHS-), 133.4 (C-2), 122.3 (C-25), 121.0 (C-16), 113.8 (-S<u>C</u>H=CHN=), 83.7 (C-15), 81.5 (C-14), 79.4 (C-22), 72.3 (C-4), 61.5 (C-5), 60.3 (C-6), 54.8 (C-13), 47.8 (C-10), 39.6 (C-9), 37.4 (C-12), 35.8 (C-20), 35.5 (C-8), 34.5 (C-23), 33.1 (-NHCO<u>C</u>H$_2$-), 30.9 (-OCO<u>C</u>H$_2$-), 24.5 (C-7), 21.5 (C-11), 21.4 (-CO<u>C</u>H$_3$), 20.6 (C-28), 17.8 (C-21), 16.0 (C-19), 16.0 (C-18), 12.6 (C-27). HRMS m/z calculated for $C_{37}H_{44}N_2O_{10}S$, 708.2717; found $[M + H]^+$, 709.2761.

*4.1.6.10. (20S, 22R)-15α-acetoxy-5β,6β-epoxy-14β-dihydroxy-1-oxowitha-2,16,24-trienolide-4β-yl 4-(benzo[d]thiazol-2-ylamino)-4-oxobutanoate (**10**).* Pale yellow amorphous powder. Yield: 17.3 mg (60.0%). ^{1}H NMR (500 MHz, $CDCl_3$), The hydrogen signals of the benzene ring [δ 7.82 (1H, d, *J* = 7.9 Hz), 7.76 (1H, d, *J* = 8.1 Hz), 7.44 (1H, t, *J* = 7.6 Hz), 7.32 (1H, t, *J* = 7.5 Hz)], 7.02 (1H, dd, *J* = 9.8, 6.0 Hz, H-3), 6.23 (1H, d, *J*=9.8 Hz, H-2), 5.68 (1H, d, *J*=2.6 Hz, H-16), 5.21 (1H, d, *J*=2.7 Hz, H-15), 4.79 (1H , d, *J* = 6.0 Hz, H-4), 4.23 (1H, ddd, *J*=12.5, 6.6, 3.5 Hz, H-22), 3.35(1H, s, H-6), 1.93 (3H, s, -COC<u>H</u>$_3$), 1.91 (3H, s, Me-28), 1.85 (3H, s, Me-27), 1.35 (3H, s, Me-19), 1.11 (3H, d, *J* = 7.0 Hz, Me-21), 1.07 (3H, s, Me-18). ^{13}C NMR (126 MHz, $CDCl_3$), δ 201.4 (C-1), 171.5 (-<u>C</u>ONH-), 170.0 (-<u>C</u>OO-), 169.7 (-<u>C</u>OCH$_3$), 166.3 (C-26), 162.4 (C-17), 159.0 (-S<u>C</u>=N-), 148.7 (C-24), 140.1 (C-3), 133.5 (C-2), 122.3 (C-25), 121.0 (C-16), The carbon signals of the benzene ring [147.7, 131.9, 126.6, 124.2, 121.7, 120.7], 83.7 (C-15), 81.6 (C-14), 79.3 (C-22), 72.3 (C-4), 61.4 (C-5), 60.4 (C-6), 52.1 (C-13), 47.9 (C-10), 39.6 (C-9), 37.3 (C-12), 35.4 (C-20), 34.6 (C-8), 32.9 (C-23), 31.1 (-NHCO<u>C</u>H$_2$-), 28.8 (-OCO<u>C</u>H$_2$-), 24.5 (C-7), 21.5 (C-11), 21.1 (-CO<u>C</u>H$_3$), 20.6 (C-28), 17.7

(C-21), 16.0 (C-19), 15.9 (C-18), 12.6 (C-27). HRMS m/z calculated for $C_{41}H_{46}N_2O_{10}S$, 758.2873; found $[M + H]^+$, 759.2940.

*4.1.6.11. (20S, 22R)-15α-acetoxy-5β,6β-epoxy-14β-dihydroxy-1-oxowitha-2,16,24-trienolide-4β-yl 4-((4-fluorophenyl)amino)-4-oxobutanoate (**11**).* Pale yellow amorphous powder. Yield: 12.2 mg (44.5%). ^{1}H NMR (500 MHz, $CDCl_3$), The hydrogen signals of the phenyl ring [δ 7.61 (2H, m), 7.14 (2H, m)], 6.97 (1H, m, H-3), 6.18 (1H, d, J = 9.8 Hz, H-2), 5.66 (1H, d, J = 2.3 Hz, H-16), 5.21 (1H, d, J = 2.6 Hz, H-15), 4.78 (1H , d, J = 6.2 Hz, H-4), 4.22 (1H, m, H-22), 1.97 (3H, s, -COC<u>H</u>$_3$), 1.92 (3H, s, Me-28), 1.83 (3H, s, Me-27), 1.39 (3H, s, Me-19), 1.09 (3H, d, J = 7.0 Hz, Me-21), 1.06 (3H, s, Me-18). ^{13}C NMR (126 MHz, $CDCl_3$), δ 202.7 (C-1), 176.2 (-<u>C</u>ONH-), 172.1(-<u>C</u>OO-), 169.9 (-<u>C</u>OCH$_3$), 166.4 (C-26), 162.5 (C-17), 148.7 (C-24), 140.1 (C-3), 133.4 (C-2), 122.3 (C-25), 121.0 (C-16), The carbon signals of the phenyl ring [142.8, 131.6, 128.5, 128.4, 116.4, 116.3], 83.7 (C-15), 81.6 (C-14), 79.5 (C-22), 72.1 (C-4), 69.7 (C-5), 63.5 (C-6), 52.2 (C-13), 51.0 (C-10), 39.4 (C-9), 37.6 (C-12), 35.5 (C-20), 34.8 (C-8), 34.6 (C-23), 33.1 (-NHCO<u>C</u>H$_2$-), 32.1 (-OCO<u>C</u>H$_2$-), 24.8 (C-7), 22.0 (C-11), 21.5 (-CO<u>C</u>H$_3$), 20.6 (C-28), 17.8 (C-21), 17.6 (C-19), 16.0 (C-18), 12.6 (C-27). HRMS m/z calculated for $C_{40}H_{46}FNO_{10}$, 719.3106; found $[M + Na]^+$, 742.2958.

*4.1.6.12. (20S, 22R)-15α-acetoxy-5β,6β-epoxy-14β-dihydroxy-1-oxowitha-2,16,24-trienolide-4β-yl 4-((4-(dimethylamino)phenyl)amino)-4-oxobutanoate (**12**).* Yellow amorphous powder. Yield: 9.6 mg (34.1%). ^{1}H NMR (500 MHz, $CDCl_3$), The hydrogen signals of the phenyl ring [δ 7.09 (2H, d, J = 9.1 Hz), 6.75 (2H, d, J = 9.0 Hz)], 6.95 (1H, dd, J = 10.0, 5.7 Hz, H-3), 6.18 (1H, d, J = 10.0 Hz, H-2), 5.68 (1H, d, J = 2.6 Hz, H-16), 5.23 (1H, d, J = 2.6 Hz, H-15), 4.23 (1H, ddd, J = 12.4, 6.9, 3.5 Hz, H-22), 3.81 (1H , d, J = 5.7 Hz, H-4), 3.37 (1H, s, H-6), 2.97

(6H, s, -N(-C<u>H</u>$_3$)), 2.86 (4H, m, -(C<u>H</u>$_2$)$_2$-), 1.95 (3H, s, -COC<u>H</u>$_3$), 1.93 (3H, s, Me-28), 1.85 (3H, s, Me-27), 1.42 (3H, s, Me-19), 1.12 (3H, d, *J* = 7.0 Hz, Me-21), 1.09 (3H, s, Me-18). ^{13}C NMR (126 MHz, $CDCl_3$), *δ* 202.7 (C-1), 177.0 (-NH-<u>C</u>O-), 169.9 (-<u>C</u>OCH$_2$-), 166.3 (-<u>C</u>OCH$_3$), 162.6 (C-26), 150.6 (C-17), 148.6 (C-24), 142.8(C-3), 131.6 (C-2), 122.3 (C-25), 121.0 (C-16), The carbon signals of the phenyl ring [148.6, 127.3, 127.3, 120.4, 112.6, 112.6], 83.7 (C-15), 81.6 (C-14), 79.5 (C-22), 69.7 (C-4), 63.6, (C-5), 63.3 (C-6), 52.2 (C-13), 47.7 (C-10), 40.6 (-N(-<u>C</u>H$_3$)$_2$), 40.6 (-N(-<u>C</u>H$_3$)$_2$), 39.4 (C-9), 37.6 (C-12), 35.5 (C-20), 34.8 (C-8), 33.1 (C-23), 28.5 (-<u>C</u>H$_2$-), 28.5 (-<u>C</u>H$_2$-), 24.8 (C-7), 22.1 (C-11), 21.5 (-CO<u>C</u>H$_3$), 20.6 (C-28), 17.8 (C-21), 17.6 (C-19), 16.0 (C-18), 12.6 (C-27). HRMS m/z calculated for $C_{42}H_{52}N_2O_{10}$, 744.3622; found $[M + H]^+$, 745.3597.

*4.1.6.13. (20S, 22R)-15α-acetoxy-5β,6β-epoxy-14β-dihydroxy-1-oxowitha-2,16,24-trienolide-4β-yl 4-((4-methoxyphenyl)amino)-4-oxobutanoate (**13**).* Pale yellow amorphous powder. Yield: 15.6 mg (56.0%). ^{1}H NMR (500 MHz, $CDCl_3$), *δ* 7.45 (1H, s, -CON<u>H</u>-), The hydrogen signals of the phenyl ring [*δ* 7.40 (2H, d, *J* = 8.9 Hz), 6.84 (2H, d, *J* = 8.9 Hz)], 7.01 (1H, dd, *J* = 9.8, 6.0 Hz, H-3), 6.23 (1H, d, *J* = 9.8 Hz, H-2), 5.68 (1H, d, *J* = 2.5 Hz, H-16), 5.21 (1H, d, *J* = 2.6 Hz, H-15), 4.80 (1H , d, *J* = 6.0 Hz, H-4), 4.23 (1H, ddd, *J* = 12.3, 6.7, 3.4 Hz, H-22), 3.35 (1H, s, H-6), 1.93 (3H, s, -COC<u>H</u>$_3$), 1.93 (3H, s, Me-28), 1.85 (3H, s, Me-27), 1.39 (3H, s, Me-19), 1.11 (3H, d, *J* = 7.0 Hz, Me-21), 1.08 (3H, s, Me-18). ^{13}C NMR (126 MHz, $CDCl_3$), *δ* 201.5 (C-1), 172.1 (-<u>C</u>ONH-), 169.7 (-<u>C</u>OO-), 169.1 (-<u>C</u>OCH$_3$), 166.3 (C-26), 162.4 (C-17), 148.6 (C-24), 140.2 (C-3), 133.4 (C-2), 122.3 (C-25), 121.0 (C-16), The carbon signals of the phenyl ring [156.5, 131.1, 121.9, 121.9, 114.2, 114.2], 83.7 (C-15), 81.6 (C-14), 79.4 (C-22), 72.0 (C-4), 61.5 (C-5), 60.5 (C-6), 55.6 (-O<u>C</u>H$_3$), 52.2 (C-13), 48.0 (C-10), 39.6 (C-9), 37.4 (C-12), 35.5 (-NHCO<u>C</u>H$_2$-), 34.6 (C-20), 33.0 (C-8), 32.1 (C-23), 29.7 (-OCO<u>C</u>H$_2$-), 24.5 (C-7), 21.5 (C-11), 21.2 (-CO<u>C</u>H$_3$), 20.6 (C-28), 17.7 (C-21), 16.0

(C-19), 16.0 (C-18), 12.6 (C-27). HRMS m/z calculated for $C_{41}H_{49}NO_{11}$, 731.3306; found $[M + Na]^+$, 754.3168.

*4.1.6.14. (20S, 22R)-15α-acetoxy-5β,6β-epoxy-14β-dihydroxy-1-oxowitha-2,16,24-trienolide-4β-yl 4-((3-fluoro-4-morpholinophenyl)amino)-4-oxobutanoate (**14**).* Pale yellow amorphous powder. Yield: 15.3 mg (50.0%). ^{1}H NMR (500 MHz, $CDCl_3$), The hydrogen signals of the phenyl ring [δ 7.03 (2H, t, J = 8.6 Hz), 6.94 (2H, dd, J = 8.9, 4.5 Hz)], 7.10 (1H, dd, J = 9.8, 6.0 Hz, H-3), 6.29 (1H, d, J = 9.8 Hz, H-2), 5.73 (1H, d, J = 2.3 Hz, H-16), 5.27 (1H, d, J = 2.5 Hz, H-15), 4.82 (1H , d, J = 6.0 Hz, H-4), 4.28 (1H, ddd, J = 10.7, 6.6, 3.3 Hz, H-22), 3.80 (4H, t, J = 4.1 Hz, O($C\underline{H}_2$-)$_2$), 3.06 (4H, t, J = 3.8 Hz, -N($C\underline{H}_2$-)$_2$), 1.95 (3H, s, -COC$\underline{H}_3$), 1.94 (3H, s, Me-28), 1.86 (3H, s, Me-27), 1.35 (3H, s, Me-19), 1.12 (3H, d, J = 7.0 Hz, Me-21), 1.07 (3H, s, Me-18). ^{13}C NMR (126 MHz, $CDCl_3$), δ 201.4 (C-1), 172.1 (-$\underline{C}$ONH-), 169.7 (-$\underline{C}$OO-), 169.3 (-$\underline{C}$OCH_3), 166.2 (C-26), 162.5 (C-17), 148.5 (C-24), 140.5 (C-3), 133.3 (C-2), 122.4 (C-25), 121.1 (C-16), The carbon signals of the phenyl ring [156.8, 147.8, 118.8, 118.8, 115.9, 115.8], 83.8 (C-15), 81.6 (C-14), 79.4 (C-22), 72.0 (C-4), 67.1 (C-5), 61.2 (C-6), 52.2 (C-13), 50.8 (-O$\underline{C}$HCHN-), 50.5 (-O$\underline{C}$HCHN-), 48.0 (C-10), 45.4 (-N$\underline{C}$HCHO-), 41.9 (-N$\underline{C}$HCHO-), 39.6 (C-9), 37.4 (C-12), 35.5 (C-20), 34.5 (C-8), 33.1 (C-23), 29.4 (-NHCO$\underline{C}H_2$-), 28.1 (-OCO$\underline{C}H_2$-), 24.6 (C-7), 21.5 (C-11), 21.1 (-CO$\underline{C}H_3$), 20.6.0 (C-28), 17.7 (C-21), 16.0 (C-19), 15.9 (C-18), 12.6 (C-27). HRMS m/z calculated for $C_{44}H_{53}FN_2O_{11}$, 804.3633; found $[M + H]^+$, 805.3667.

*4.1.6.15. (20S, 22R)-15α-acetoxy-5β,6β-epoxy-14β-dihydroxy-1-oxowitha-2,16,24-trienolide-4β-yl 4-((1,3,4-thiadiazol-2-yl)amino)-4-oxobut-2-enoate (**15**).* Pale yellow amorphous powder. Yield: 12.4 mg (46.0%). ^{1}H NMR (600 MHz, $CDCl_3$), δ 8.97 (1H, s, -SC$\underline{H}$=N-), 7.54 (1H, d,

J = 15.5 Hz, -CH=CH-), 7.12 (2H, m, -CH=CH-), 7.12 (2H, m, H-3), 6.33 (1H, d, *J* = 9.8 Hz, H-2), 5.69 (1H, d, *J* = 2.5 Hz, H-16), 5.23 (1H, d, *J* = 2.6 Hz, H-15), 4.92 (1H , d, *J* = 6.1 Hz, H-4), 4.23 (1H, ddd, *J* = 12.4, 6.7, 3.4 Hz, H-22), 3.49 (1H, s, H-6), 1.96 (3H, s, -COCH_3), 1.93 (3H, s, Me-28), 1.86 (3H, s, Me-27), 1.44 (3H, s, Me-19), 1.12 (3H, d, *J* = 7.0 Hz, Me-21), 1.09 (3H, s, Me-18). ^{13}C NMR (151 MHz, $CDCl_3$), *δ* 201.3 (C-1), 164.1 (-CONH-), 161.9 (-COO-), 169.7 (-$COCH_3$), 166.3 (C-26), 162.5 (C-17), 160.2 (-SCN-NH-), 148.7 (C-24), 148.5 (-SCHN-), 139.8 (C-3), 134.9 (-CH=CH-), 134.0 (-CH=CH-), 133.1 (C-2), 122.3 (C-25), 121.0 (C-16), 83.7 (C-15), 81.6 (C-14), 79.4 (C-22), 73.05 (C-4), 61.4 (C-5), 60.3 (C-6), 52.2 (C-13), 48.1 (C-10), 39.7 (C-9), 37.4 (C-12), 35.5 (C-20), 34.5 (C-8), 33.1 (C-23), 29.3 (C-7), 27.4 (C-11), 21.5 (-COCH_3), 20.6 (C-28), 17.8 (C-21), 16.0 (C-19), 15.9 (C-18), 12.6 (C-27). HRMS m/z calculated for $C_{36}H_{41}N_3O_{10}S$, 707.2513; found $[M + Na]^+$, 730.0628.

*4.1.6.16. (20S, 22R)-15α-acetoxy-5β,6β-epoxy-14β-dihydroxy-1-oxowitha-2,16,24-trienolide-4β-yl 4-(thiazol-2-ylamino)-4-oxobut-2-enoate (**16**).* Pale yellow amorphous powder. Yield: 11.8 mg (43.9%). ^{1}H NMR (500 MHz, $CDCl_3$), δ 7.48 (1H, d, *J* = 7.2 Hz, =NCH=CHS-), 7.02 (1H, m, H-3), 7.01 (1H, d, *J*=6.0 Hz, -SCH=CHN=), 6.24 (1H, d, *J*=9.8 Hz, H-2), 5.68 (1H, d, *J*=2.1 Hz, H-16), 5.21 (1H, d, *J*=2.7 Hz, H-15), 4.89 (1H , d, *J* = 6.0 Hz, H-4), 4.23 (1H, ddd, *J*=12.3, 6.8, 3.4 Hz, H-22), 3.41 (1H, s, H-6), 1.95 (3H, s, -COCH_3), 1.93 (3H, s, Me-28), 1.86 (3H, s, Me-27), 1.41 (3H, s, Me-19), 1.11 (3H, d, *J* = 7.0 Hz, Me-21), 1.08 (3H, s, Me-18). ^{13}C NMR (126 MHz, $CDCl_3$), δ 201.2 (C-1), 171.4 (-CONH-), 170.1 (-COO-), 169.7 (-$COCH_3$), 166.4 (C-26), 162.4 (C-17), 159.8 (-N=C-S-), 148.6 (C-24), 140.1 (C-3), 134.7 (=NCH=CHS-), 133.4 (C-2), 122.3 (C-25), 121.0 (C-16), 113.8 (-SCH=CHN=), 83.7 (C-15), 81.5 (C-14), 79.4 (C-22), 72.3 (C-4), 61.5 (C-5), 60.3 (C-6), 54.8 (C-13), 47.8 (C-10), 39.6 (C-9), 37.4 (C-12), 35.8 (C-20), 35.5 (C-8), 34.5 (C-23), 33.1 (-NHCOCH_2-), 30.9

(-OCO<u>C</u>H_2-), 24.5 (C-7), 21.5 (C-11), 21.4 (-CO<u>C</u>H_3), 20.6 (C-28), 17.8 (C-21), 16.0 (C-19), 16.0 (C-18), 12.6 (C-27). HRMS m/z calculated for $C_{37}H_{42}N_2O_{10}S$, 706.2560; found [M + Na]$^+$, 729.2412.

*4.1.6.17. (20S, 22R)-15α-acetoxy-5β,6β-epoxy-14β-dihydroxy-1-oxowitha-2,16,24-trienolide-4β-yl 4-(benzo[d]thiazol-2-ylamino)-4-oxobut-2-enoate (**17**).* Pale yellow amorphous powder. Yield: 10.6 mg (36.9%). ^{1}H NMR (500 MHz, $CDCl_3$), The hydrogen signals of the benzene ring [δ 7.85 (1H, d, *J* = 7.8 Hz), 7.77 (1H, d, *J* = 8.1 Hz), 7.47 (1H, t, *J* = 7.7 Hz), 7.35 (1H, t, *J* = 7.6 Hz)], 7.14 (1H, d, *J*=15.4 Hz, -C<u>H</u>=CH-), 7.09 (1H, dd, *J* = 9.8, 6.1 Hz, H-3), 7.05 (1H, d, *J*=15.4 Hz, -CH=C<u>H</u>-), 6.31 (1H, d, *J*=9.8 Hz, H-2), 5.69 (1H, d, *J*=2.5 Hz, H-16), 5.23 (1H, d, *J*=2.6 Hz, H-15), 4.91 (1H , d, *J* = 6.1 Hz, H-4), 4.23 (1H, ddd, *J*=12.5, 6.5, 3.5 Hz, H-22), 3.41(1H, s, H-6), 1.95 (3H, s, -COC<u>H</u>$_3$), 1.93 (3H, s, Me-28), 1.87 (3H, s, Me-27), 1.42 (3H, s, Me-19), 1.12 (3H, d, *J* = 7.0 Hz, Me-21), 1.09 (3H, s, Me-18). ^{13}C NMR (126 MHz, $CDCl_3$), δ 201.1 (C-1), 171.5 (-<u>C</u>ONH-), 169.7 (-<u>C</u>OO-), 169.7 (-<u>C</u>OCH_3), 164.1 (C-26), 162.4 (C-17), 161.6 (-S<u>C</u>=N-), 148.7 (C-24), 139.5 (C-3), 135.2 (-<u>C</u>H=CH-), 134.1 (C-2), 126.7(-CH=<u>C</u>H-), 122.3 (C-25), 121.0 (C-16), The carbon signals of the benzene ring [132.6, 129.9, 124.6, 121.7, 121.1, 121.0], 83.7 (C-15), 81.6 (C-14), 79.4 (C-22), 73.1 (C-4), 61.4 (C-5), 60.4 (C-6), 52.2 (C-13), 48.0 (C-10), 39.7 (C-9), 37.3 (C-12), 35.4 (C-20), 34.6 (C-8), 32.9 (C-23), 24.5 (C-7), 21.5 (C-11), 21.1 (-CO<u>C</u>H_3), 20.6 (C-28), 17.6 (C-21), 16.0 (C-19), 14.3 (C-18), 12.6 (C-27). HRMS m/z calculated for $C_{41}H_{44}N_2O_{10}S$, 756.2717; found [M + Na]$^+$, 779.2569.

*4.1.6.18. (20S, 22R)-15α-acetoxy-5β,6β-epoxy-14β-dihydroxy-1-oxowitha-2,16,24-trienolide-4β-yl 4-((4-fluorophenyl)amino)-4-oxobut-2-enoate (**18**).* Pale yellow amorphous powder. Yield:

10.7 mg (39.2%). ^{1}H NMR (500 MHz, $CDCl_3$), The hydrogen signals of the phenyl ring [δ 7.63 (2H, m), 7.04 (2H, m)], 7.04 (1H, m, H-3), 6.98 (1H, d, *J* = 15.2 Hz, -C<u>H</u>=CH-), 6.89 (1H, d, *J* = 15.3 Hz, -C<u>H</u>=CH-), 6.31 (1H, d, *J* = 9.8 Hz, H-2), 5.66 (1H, d, *J* = 2.3 Hz, H-16), 5.18 (1H, d, *J* = 2.6 Hz, H-15), 4.90 (1H , d, *J* = 6.2 Hz, H-4), 4.21 (1H, m, H-22), 1.95 (3H, s, -COC<u>H</u>$_3$), 1.94 (3H, s, Me-28), 1.89 (3H, s, Me-27), 1.44 (3H, s, Me-19), 1.09 (3H, d, *J* = 7.0 Hz, Me-21), 1.02 (3H, s, Me-18). ^{13}C NMR (151 MHz, $CDCl_3$), δ 200.9 (C-1), 169.7 (-<u>C</u>OCH$_3$), 167.3 (C-26), 164.6 (-<u>C</u>ONH-), 161.8 (C-17), 161.2 (-<u>C</u>OO-), 149.9 (C-24), 139.5 (C-3), 138.2 (-CH=CH-), 134.2 (C-2), 130.0 (-CH=CH-), 122.0 (C-25), 121.1 (C-16), The carbon signals of the phenyl ring [121.9, 121.9, 121.9, 121.9, 116.0, 116.0, 115.8, 115.8], 83.7 (C-15), 81.4 (C-14), 79.0 (C-22), 72.0 (C-4), 61.4 (C-5), 61.2 (C-6), 52.22 (C-13), 48.0 (C-10), 39.8 (C-9), 37.1 (C-12), 35.3 (C-20), 35.0 (C-8), 32.0 (C-23), 24.5 (C-7), 21.5 (C-11), 20.8 (-CO<u>C</u>H$_3$), 20.7 (C-28), 17.0 (C-21), 15.9 (C-19), 15.7 (C-18), 12.6 (C-27). HRMS m/z calculated for $C_{40}H_{44}FNO_{10}$, 717.2949; found $[M + Na]^+$, 740.2816.

*4.1.6.19. (20S, 22R)-15α-acetoxy-5β,6β-epoxy-14β-dihydroxy-1-oxowitha-2,16,24-trienolide-4β-yl 4-((4-(dimethylamino)phenyl)amino)-4-oxobut-2-enoate (**19**).* Yellow amorphous powder. Yield: 10.0 mg (35.5%). ^{1}H NMR (600 MHz, $CDCl_3$), The hydrogen signals of the phenyl ring [δ 7.49 (2H, d, *J* = 9.0 Hz), 6.70 (2H, d, *J* = 9.1 Hz)], 7.04 (1H, dd, *J* = 9.8, 6.1 Hz, H-3), 6.97 (1H, d, *J* = 15.2 Hz, -C<u>H</u>=CH-), 6.86 (1H, d, *J* = 15.2 Hz, -C<u>H</u>=CH-), 6.29 (1H, d, *J* = 9.8 Hz, H-2), 5.66 (1H, d, *J* = 2.6 Hz, H-16), 5.20 (1H, d, *J* = 2.7 Hz, H-15), 4.87 (1H , d, *J* = 6.1 Hz, H-4), 4.23 (1H, ddd, *J* = 12.6, 6.3, 3.5 Hz, H-22), 2.93 (6H, s, -N(-C<u>H</u>$_3$)), 1.94 (3H, s, -COC<u>H</u>$_3$), 1.94 (3H, s, Me-28), 1.87 (3H, s, Me-27), 1.43 (3H, s, Me-19), 1.10 (3H, d, *J* = 7.0 Hz, Me-21), 1.06 (3H, s, Me-18). ^{13}C NMR (151 MHz, $CDCl_3$), δ 201.2 (C-1), 169.7 (-<u>C</u>OCH$_3$), 166.8 (C-26), 164.8 (-<u>C</u>ONH-), 162.1 (C-17), 160.7 (-<u>C</u>OO-), 149.2 (C-24), 139.8 (C-3), 138.4 (-CH=CH-), 134.0 (C-2), 129.3 (-CH=CH-), 122.1 (C-25), 121.0 (C-16), The

carbon signals of the phenyl ring [148.4, 127.4, 121.7, 121.7, 112.9, 112.9], 83.7 (C-15), 81.5 (C-14), 79.1 (C-22), 72.5 (C-4), 61.3 (C-5), 60.7 (C-6), 52.2 (C-13), 48.0 (C-10), 40.9 (-N-CH_3), 40.9 (-N-CH_3), 39.7 (C-9), 37.3 (C-12), 35.4 (C-20), 34.8 (C-8), 32.6 (C-23), 24.5 (C-7), 21.5 (C-11), 20.9 (-COCH_3), 20.6 (C-28), 17.4 (C-21), 15.9 (C-19), 15.9 (C-18), 12.6 (C-27). HRMS m/z calculated for $C_{42}H_{50}N_2O_{10}$, 742.3465; found $[M + H]^+$, 743.3504.

*4.1.6.20. (20S, 22R)-15α-acetoxy-5β,6β-epoxy-14β-dihydroxy-1-oxowitha-2,16,24-trienolide-4β-yl 4-((4-methoxyphenyl)amino)-4-oxobut-2-enoate (**20**).* Pale yellow amorphous powder. Yield: 7.8 mg (28.2%). ^{1}H NMR (500 MHz, $CDCl_3$), δ 8.37 (1H, s, -CONH-), The hydrogen signals of the phenyl ring [7.59 (2H, d, J = 8.7 Hz), 6.86 (2H, d, J = 8.7 Hz)], 7.03 (1H, dd, J = 9.6, 6.2 Hz, H-3), 6.97 (1H, d, J = 15.2 Hz, -CH=CH-), 6.88 (1H, d, J = 15.2 Hz, -CH=CH-),6.31 (1H, d, J = 9.8 Hz, H-2), 5.65 (1H, s, H-16), 5.17 (1H, s, H-15), 4.90 (1H , d, J = 6.0 Hz, H-4), 4.2 (1H, m, H-22), 3.41 (1H, s, H-6), 1.95 (3H, s, -COCH_3), 1.94 (3H, s, Me-28), 1.89 (3H, s, Me-27), 1.44 (3H, s, Me-19), 1.09 (3H, d, J = 7.0 Hz, Me-21), 1.02 (3H, s, Me-18). ^{13}C NMR (126 MHz, $CDCl_3$), δ 200.8 (C-1), 169.7 (-CONH-), 167.3 (-COO-), 164.7 (-COCH_3), 161.7 (C-26), 160.9 (C-17), 149.9 (C-24), 139.5 (C-3), 138.5 (-CH=CH-), 134.2 (C-2), 129.5 (-CH=CH-), 122.0 (C-25), 121.2 (C-16), The carbon signals of the phenyl ring [156.9, 131.0, 121.8, 121.8, 114.3, 114.3], 83.6 (C-15), 81.4 (C-14), 78.9 (C-22), 72.3 (C-4), 61.5 (C-5), 61.3 (C-6), 55.6 (-OCH_3), 52.2 (C-13), 48.0 (C-10), 39.9 (C-9), 37.0 (C-12), 35.2 (C-20), 35.0 (C-8), 31.8 (C-23), 24.5 (C-7), 21.5 (C-11), 20.8 (-COCH_3), 20.7 (C-28), 16.9 (C-21), 16.0 (C-19), 15.7 (C-18), 12.6 (C-27). HRMS m/z calculated for $C_{41}H_{47}NO_{11}$, 729.3149; found $[M + Na]^+$, 752.2988.

4.1.6.21. (20S, 22R)-15α-acetoxy-5β,6β-epoxy-14β-dihydroxy-1-oxowitha-2,16,24-trienolide-4β-yl

*4-((3-fluoro-4-morpholinophenyl)amino)-4-oxobut-2-enoate (**21**).* Pale yellow amorphous powder. Yield: 15.4 mg (50.5%). ^{1}H NMR (500 MHz, $CDCl_3$), The hydrogen signals of the phenyl ring [δ 7.59 (1H, d, *J* = 13.5 Hz), 7.29 (1H, d, *J* = 7.3 Hz), 7.03 (1H, dd, *J* = 9.8, 6.2 Hz)], 6.96 (1H, dd, *J* = 9.6, 5.9 Hz, H-3), 6.96 (1H, d, *J* = 15.3 Hz, -C<u>H</u>=CH-), 6.87 (1H, d, *J* = 15.2 Hz, -C<u>H</u>=CH-), 6.31 (1H, d, *J* = 9.8 Hz, H-2), 5.65 (1H, d, *J* = 2.4 Hz, H-16), 5.17 (1H, d, *J* = 2.6 Hz, H-15), 4.89 (1H , d, *J* = 6.2 Hz, H-4), 4.20 (1H, ddd, *J* = 12.7, 5.3, 3.7 Hz, H-22), 3.88 (4H, t, *J* = 4.2 Hz, -C<u>H</u>$_2$OC<u>H</u>$_2$-), 3.08 (4H, t, *J* = 3.9 Hz, -C<u>H</u>$_2$NC<u>H</u>$_2$-), 1.96 (3H, s, -COC<u>H</u>$_3$), 1.93 (3H, s, Me-28), 1.89 (3H, s, Me-27), 1.44 (3H, s, Me-19), 1.08 (3H, d, *J* = 7.0 Hz, Me-21), 1.01 (3H, s, Me-18). ^{13}C NMR (126 MHz, $CDCl_3$), δ 202.8 (C-1), 169.7 (-<u>C</u>OCH$_3$), 167.4 (C-26), 164.6 (-<u>C</u>ONH-), 161.7 (C-17), 161.1 (-<u>C</u>OO-), 150.0 (C-24), 139.4 (C-3), 138.2 (-CH=CH-), 134.2 (C-2), 129.9 (-CH=CH-), 121.9 (C-25), 121.1 (C-16), The carbon signals of the phenyl ring [156.2, 154.6, 116.0, 116.0, 109.2, 108.0], 83.7 (C-15), 81.4 (C-14), 79.0 (C-22), 72.3 (C-4), 67.0 (C-5), 61.5 (C-6), 61.3 (-O<u>C</u>HCHN-), 60.5 (-O<u>C</u>HCHN-), 52.2 (C-13), 51.2 (-N<u>C</u>HCHO-), 51.0 (-N<u>C</u>HCHO-), 48.0 (C-10), 39.8 (C-9), 37.1 (C-12), 35.2 (C-20), 35.0 (C-8), 31.9 (C-23), 24.4 (C-7), 21.5 (C-11), 20.8 (-CO<u>C</u>H$_3$), 20.7 (C-28), 17.0 (C-21), 16.0 (C-19), 15.7 (C-18), 12.5 (C-27). HRMS m/z calculated for $C_{44}H_{51}FN_2O_{11}$, 802.3477; found $[M + H]^+$, 803.3513.

*4.1.7. General procedure for synthesis of compounds **22-25***

EDCI·HCl (2.2 eq.), HOBt·H2O (1.5 eq.), and pyridine (3.0 eq.) were added to a solution of Acid (the intermediate **a**, **b**, **c**, or **d**; 1.0 eq.) in DMF at room temperature under N_2 atmosphere. After 30 min, a solution of R_2-H (**Scheme 2**; 2.2 eq.) in DMF was added dropwise. The mixture was then stirred for 48 h at room temperature and, upon completion of the reaction, water was added and extracted with EtOAc. The organic layers were then washed with brine, dried over Na_2SO_4, filtered and concentrated in vacuo. The residue was

purified via preparative HPLC using acetonitrile/water (1/1-3/2) as the solvent system to obtain the target compounds.

4.1.7.1.

(20S,22R)-15α-acetoxy-5β,6β-epoxy-14β-dihydroxy-1-oxowitha-2,16,24-trienolide-3-((3-fluoro-4-morpholinophenyl)amino)-4β-yl

*5-((3-fluoro-4-morpholinophenyl)amino)-5-oxopentanoate (**22**).* Pale yellow amorphous powder. Yield: 5.8 mg (15.0%). ^{1}H NMR (500 MHz, $CDCl_3$), δ 7.96 (1H, s, -CONH-), The hydrogen signals of the phenyl ring [7.63 (1H, d, *J* = 14.0 Hz), 7.10 (1H, d, *J* = 8.2 Hz), 6.92 (2H, m) 6.50 (1H, d, *J* = 14.5 Hz), 6.47 (1H, d, *J* = 8.4 Hz)], 5.72 (1H, d, *J* = 2.0 Hz, H-16), 5.25 (1H, d, *J* = 2.2 Hz, H-15), 4.79 (1H , d, *J* = 1.2 Hz, H-4), 4.22 (1H, ddd, *J* = 11.5, 7.3, 3.4 Hz, H-22), 3.86 (8H, t, *J* = 4.2 Hz, O(CH_2-)$_2$ × 2), 3.03 (8H, t, *J* = 3.9 Hz, -N(CH_2-)$_2$ × 2), 1.95 (3H, s, -COCH_3), 1.94 (3H, s, Me-28), 1.86 (3H, s, Me-27), 1.32 (3H, s, Me-19), 1.13 (3H, d, *J* = 7.0 Hz, Me-21), 1.05 (3H, s, Me-18). ^{13}C NMR (126 MHz, $CDCl_3$), δ 210.5 (C-1), 172.4 (-CONH-), 170.4 (-COO-), 169.6 (-$COCH_3$), 166.1 (C-26), 163.0 (C-17), 148.5 (C-24), 122.4 (C-25), 120.8 (C-16), The carbon signals of the phenyl ring [157.5, 156.0, 131.0, 130.0, 127.7, 116.5, 115.5, 109.7, 109.0, 108.8, 103.8, 103.1], 83.9 (C-15), 81.4 (C-14), 79.8 (C-22), 76.3 (C-4), 67.1 (C-5), 67.1 (C-6), 62.6 (-OCHCHN-), 62.3 (-OCHCHN-), 51.8 (-OCHCHN-), 51,8 (-OCHCHN-), 53.8 (C-3), 52.2 (C-13), 51.3 (-NCHCHO-), 51.3 (-NCHCHO-), 51.1 (-NCHCHO-), 51.1 (-NCHCHO-), 45.9 (C-10), 40.0 (C-9), 38.1 (C-12), 37.6 (C-2), 36.4 (C-20), 35.6 (C-8), 34.0 (C-23), 33.9 (-NHCOCH_2-), 33.4 (-OCOCH_2-), 24.7 (C-7), 22.1 (C-11), 21.7 (-COCH_3), 21.5 (-$CH_2CH_2CH_2$-), 20.6 (C-28), 17.9 (C-21), 16.2 (C-19), 16.0 (C-18), 12.6 (C-27). HRMS m/z calculated for $C_{55}H_{68}F_2N_4O_{12}$, 1014.4802; found $[M + H]^+$, 1015.4867.

4.1.7.2.

*(20S,22R)-15α-acetoxy-5β,6β-epoxy-14β-dihydroxy-1-oxowitha-2,16,24-trienolide-3-((4-met hoxyphenyl)amino)-4β-yl 5-((4-methoxyphenyl)amino)-5-oxopentanoate (**23**).* Pale yellow amorphous powder. Yield: 20.5 mg (62.0%). ^{1}H NMR (500 MHz, $CDCl_3$), δ 7.88 (1H, s, -CONH-), The hydrogen signals of the phenyl ring [7.48 (2H, d, *J* = 9.0 Hz), 6.84 (2H, d, *J* = 9.0 Hz), 6.80 (2H, d, *J* = 8.9 Hz), 6.69 (2H, d, *J* = 8.8 Hz)], 5.70 (1H, d, *J* = 2.6 Hz, H-16), 5.24 (1H, d, *J* = 2.7 Hz, H-15), 4.82 (1H , d, *J* = 2.8 Hz, H-4), 4.23 (1H, ddd, *J* =12.4, 6.9, 3.5 Hz, H-22), 3.86 (1H, m, H-3), 3.76 (3H, s, -Ph-O-CH_3), 3.74 (3H, s, -Ph-O-CH_3), 3.24 (1H, s, H-6), 2.05 (3H, s, -COCH_3), 1.93 (3H, s, Me-28), 1.85 (3H, s, Me-27), 1.30 (3H, s, Me-19), 1.12 (3H, d, *J* = 7.0 Hz, Me-21), 1.04 (3H, s, Me-18). ^{13}C NMR (126 MHz, $CDCl_3$), δ 210.7 (C-1), 172.5 (-CONH-), 170.3 (-COO-), 169.7 (-$COCH_3$), 166.2 (C-26), 162.7 (C-17), 148.6 (C-24), 122.3 (C-25), 121.0 (C-16), The carbon signals of the phenyl ring [156.4, 153.8, 139.0, 131.5, 121.6, 121.6, 116.0, 116.0, 115.3, 115.3, 114.3, 114.3], 83.9 (C-15), 81.4 (C-14), 79.5 (C-22), 76.6 (C-4), 62.2 (C-5), 55.8 (C-6), 55.6 (-OCH_3), 52.2 (C-13), 51.6 (C-3), 51.0 (C-2), 40.2 (C-10), 38.1 (C-9), 37.5 (C-12), 36.3 (-NHCOCH_2-), 35.5 (C-20), 34.1 (C-8), 33.9 (C-23), 33.1 (-OCOCH_2-), 24.6 (C-7), 21.0 (C-11), 21.6 (-COCH_3), 21.5 (-CH_2-CH_2-CH_2-), 20.6 (C-28), 17.7 (C-21), 16.1 (C-19), 15.9 (C-18), 12.6 (C-27). HRMS m/z calculated for $C_{49}H_{60}N_2O_{12}$, 868.4146; found $[M + H]^+$, 869.4184.

4.1.7.3.

*(20S,22R)-15α-acetoxy-5β,6β-epoxy-14β-dihydroxy-1-oxowitha-2,16,24-trienolide-3-((4-met hoxyphenyl)amino)-4β-yl 4-((4-methoxyphenyl)amino)-4-oxobutanoate (**24**).* Pale yellow amorphous powder. Yield: 17.6 mg (54.2%). ^{1}H NMR (500 MHz, $CDCl_3$), δ 7.53 (1H, s, -CONH-), The hydrogen signals of the phenyl ring [7.44 (2H, d, *J* =8.9 Hz), 6.85 (2H, d, *J* = 8.9 Hz), 6.76 (2H, d, *J* = 8.8 Hz), 6.62 (2H, d, *J* = 8.8 Hz)], 5.70 (1H, d, *J* = 2.5 Hz, H-16), 5.24 (1H, d, *J* = 2.6 Hz, H-15), 4.79 (1H , d, *J* = 2.6 Hz, H-4), 4.23 (1H, ddd, *J* =12.4, 6.6, 3.5

Hz, H-22), 3.84 (1H, m, H-3), 3.78 (3H, s, -Ph-O-C<u>H</u>$_3$), 3.72 (3H, s, -Ph-O-C<u>H</u>$_3$), 3.21 (1H, s, H-6), 2.02 (3H, s, -COC<u>H</u>$_3$), 1.93 (3H, s, Me-28), 1.85 (3H, s, Me-27), 1.34 (3H, s, Me-19), 1.12 (3H, d, *J* = 7.0 Hz, Me-21), 1.06 (3H, s, Me-18). ^{13}C NMR (126 MHz, $CDCl_3$), δ 210.5 (C-1), 171.7 (-<u>C</u>ONH-), 169.6 (-<u>C</u>OO-), 169.2 (-<u>C</u>OCH$_3$), 166.3 (C-26), 162.5 (C-17), 148.7 (C-24), 122.3 (C-25), 121.1 (C-16), The carbon signals of the phenyl ring [139.03, 131.13, 127.96, 121.80, 121.80, 115.95, 115.3, 115.3, 114.3, 114.3, 156.5, 153.7], 83.9 (C-15), 81.5 (C-14), 79.3 (C-22), 76.8 (C-4), 61.45 (C-5), 55.8 (C-6), 55.6 (-O<u>C</u>H$_3$), 52.3 (C-13), 51.3 (C-3), 51.0 (C-2), 40.5 (C-10), 38.3 (C-9), 37.4 (C-12), 35.5 (-NHCO<u>C</u>H$_2$-), 34.3 (C-20), 33.0 (C-8), 32.0 (C-23), 30.0 (-OCO<u>C</u>H$_2$-), 24.5 (C-7), 21.7 (C-11), 21.5 (-CO<u>C</u>H$_3$), 20.6 (C-28), 17.6 (C-21), 16.0 (C-19), 15.4 (C-18), 12.6 (C-27). HRMS m/z calculated for $C_{48}H_{58}N_2O_{12}$, 854.3990; found $[M + H]^+$, 855.2995.

4.1.7.4.

*(20S,22R)-15α-acetoxy-5β,6β-epoxy-14β-dihydroxy-1-oxowitha-2,16,24-trienolide-3-((4-met hoxyphenyl)amino)-4β-yl 4-((4-methoxyphenyl)amino)-4-oxobut-2-enoate (**25**).* Pale yellow amorphous powder. Yield: 19.2 mg (59.3%). ^{1}H NMR (500 MHz, $CDCl_3$), δ 7.54 (1H, s, -CON<u>H</u>-), The hydrogen signals of the phenyl ring [7.45 (2H, d, *J* = 8.6 Hz), 7.33 (2H, d, *J* = 8.6 Hz), 7.21 (2H, d, *J* = 8.5 Hz), 6.61 (2H, d, *J* = 8.5 Hz)], 5.70 (1H, d, *J* = 2.5 Hz, H-16), 5.24 (1H, d, *J* = 2.6 Hz, H-15), 4.84 (1H , d, *J* = 2.7 Hz, H-4), 4.23 (1H, ddd, *J* = 12.5, 6.6, 3.5 Hz, H-22), 3.90 (1H, m, H-3), 3.22 (1H, s, H-6), 2.03 (3H, s, -COC<u>H</u>$_3$), 1.93 (3H, s, Me-28), 1.86 (3H, s, Me-27), 1.37 (3H, s, Me-19), 1.13 (3H, d, *J* = 7.0 Hz, Me-21), 1.06 (3H, s, Me-18). ^{13}C NMR (126 MHz, $CDCl_3$), δ 210.7 (C-1), 171.7 (-<u>C</u>ONH-), 169.6 (-<u>C</u>OO-), 169.3 (-<u>C</u>OCH$_3$), 166.4 (C-26), 162.4 (C-17), 148.7 (C-24), 122.3 (C-25), 121.1 (C-16), The carbon signals of the phenyl ring [147.4, 143.0, 142.4, 135.3, 126.6, 126.6, 126.0, 126.0, 119.7, 119.6, 113.7, 113.7], 83.9 (C-15), 81.5 (C-14), 79.3 (C-22), 76.6 (C-4), 61.5 (C-5), 60.9 (C-6), 60.6 (-O<u>C</u>H$_3$), 52.2 (C-13), 51.0 (C-3), 51.7 (C-2), 40.4 (C-10), 38.3 (C-9), 37.5

(C-12), 35.4 (-NHCO<u>C</u>H_2-), 34.5 (C-20), 32.9 (C-8), 32.1 (C-23), 30.0(-OCO<u>C</u>H_2-), 24.5 (C-7), 21.8 (C-11), 21.5 (-CO<u>C</u>H_3), 20.6 (C-28), 17.6 (C-21), 16.0 (C-19), 15.6 (C-18), 12.6 (C-27). HRMS m/z calculated for $C_{48}H_{56}N_2O_{12}$, 852.3833; found $[M + Na]^+$, 875.2652.

4.2. GLS1 enzyme assay

In a 96-well black microplate (BPS Bioscience Cat # 79685) human glutaminase GLS1 activity was determined using the GLS1 Inhibitor Screening Assay Kit (BPS Bioscience Cat #79596). Experiments are carried out following the manufacturer's instructions.

4.3. Cell proliferation assay

The MDA-MB-231 cell line was purchased from the Cell Bank of Shanghai Institute of Biochemistry and Cell Biology, Chinese Academy of Sciences (Shanghai, People's Republic of China). The cells were cultured in Dulbecco's modified Eagle medium (DMEM, GIBCO, NY, USA), which were all supplemented with 10% fetal bovine serum (FBS; GIBCO, NY, USA) at 37°C with 5% CO_2.

The cytotoxic activity was evaluated using the MTT colorimetric method. Briefly, cells were seeded in a clear-bottom 96 well plate at a density of 5×10^3 cells/well in 100 μL of DMEM medium at 37°C for 24 h. After that, the cells were incubated with tested compounds or positive controls at the various concentrations for 24 h (0.078-10 μM). Then 20 μL of MTT (5 mg/mL) was added, and then the cells were incubated at 37°C for an additional 4 h. The medium was aspirated, and 150 μL of DMSO was added to each well. The absorbance was measured at 570 nm using a microplate reader (Spectramax Plus 384, Molecular Devices, Sunnyvale, CA, USA). The cytotoxic activity was expressed as the IC_{50} values. All experiments were done in triplicate and repeated at least three times. Vehicle DMSO (0.1%) was used as a negative control.

4.4. Colony formation assay

The MDA-MB-231 cells (1000 cells/ well) were seeded in a six-well plate in 2 mL of DMEM medium at 37°C. After 24 h, cells were treated with vehicle DMSO or different concentration of compound **7** or **WA** for 24 hours, after treatment, cells were cultured for two weeks. Culture medium was changed twice a week. After two weeks, the cell colonies were rinsed with PBS, fixed in 4% paraformaldehyde fix solution, and then stained with a solution of 0.05% crystal violet (Beyotime Company).

4.5. Apoptosis assays

Apoptotic cells were measured by Annexin VFITC/PI apoptosis detection kit (Beyotime Company) according to the provided protocol. Briefly, the MDA-MB-231 cells were treated with various concentrations of **7** or 0.1% DMSO for 12 h of incubation at 37°C. Then the cells were harvested and resuspended in PBS at a concentration of 1×10^5 cell/mL. After centrifuged at 1000 g for 5 min, 195 μL FITC-conjugated annexin V binding buffer, 5 μL of annexin V-FITC and 10 μL of propidium iodide (PI) were added. The mixture was incubated for 20 min at room temperature in the absence of light. Following gentle vortex, the sample was analyzed using a BD Accuri C6 flow cytometer (Becton & Dickinson Co.). The percentages of apoptotic and necrotic cell for each sample were estimated.

4.6. Western blot analysis

MDA-MB-231 cells were treated with various concentrations of 7 as indicated or 0.1% DMSO for 24 h. Then, the cells were harvested and total proteins were extracted with 1 × RIPA lysis buffer (50 mM Tris-HCl, pH 7.4, 150 mM NaCl, 0.25% deoxycholic acid, 1% NP-40, 1 mM EDTA and protease inhibitors) (Amresco, Solon, USA) and quantified by a BCA kit. Equivalent samples from the total cell lysates (80 μg per lane) were subjected to

SDS-polyacrylamide gel electrophoresis (SDS-PAGE, BioRad Laboratories, Hercules, CA), wet-transferred to PVDF membrane (BioRad Laboratories, Hercules, CA) and blotted with primary antibodies specific for caspase-3, cleaved caspase-3, caspase-9, cleaved caspase-9, and GAPDH at 4°C overnight, probed with the appropriate secondary isotype specific antibodies tagged with horseradish peroxidase (Cell Signaling Technology). Bound immunocomplexes were visualized using enhanced chemiluminescence (Millipore), which were detected using a ChemiDOC™ XRS + system (BioRad Laboratories, Hercules, CA).

4.7. Determination of intracellular glutamate levels

MDA-MB-231 cells were incubated in a CO_2 incubator at 37°C for 24 h. The cells were treated with the vehicle control (0.1% DMSO) or various concentrations of **7** as indicated for an additional 12 h. After that, the medium was removed and cells were washed three times with PBS, and 1 × RIPA lysis buffer (Amresco, Solon, USA) was added at 4°C. Then the cell lysates were subjected to Amplex® Red Glutamic Acid Assay Kit (Invitrogen) following the manufacturer's instructions.

4.8. ROS assay

For the fluorescence imaging observation of intracellular ROS levels, MDA-MB-231 cells were seeded in a clear-bottom 96 well plate which were treated with various concentrations of **7** or 0.1% DMSO for 3 h and then incubated in the dark with 10 mM of the oxidation-sensitive fluorescent probe DCFH-DA (Beyotime, Nantong, China) for 20 min at 37°C, and observed under a fluorescence microscope (LEICA DMI3000 B, Germany).

As for the quantitative detection of intracellular ROS levels, MDA-MB-231 cells grown at 37°C in a 5% CO_2 incubator were treated with various concentrations of **7** or 0.1% DMSO for 3 h and then incubated in the dark with 10 mM of the oxidation-sensitive fluorescent

probe DCFH-DA (Beyotime, Nantong, China) for 20 min at 37°C. DCFH-DA was cleaved by intracellular esterase to liberate free DCFH. The ROS levels of the cells were measured using a BD Accuri C6 flow cytometer (Becton & Dickinson Co.).

4.9. Molecular docking

The human GLS1 crystal structure (PDB code 3UO9) was obtained from the Protein Data Bank. The docking was performed with Discovery Studio Client software (version 3.0; Accelrys Software Inc.). Molecules were drawn in ChemBioOffice 2010, and energy minimized using the MM2 force field in Chemdraw 3D. And PyMOL (version 0.99; DeLano Scientific) was used to view the resulting models in which graphics were prepared.

4.10. In vivo xenograft model

Five-week-old male BALB/c nude mice were purchased from the Model Animal Research Center of Nanjing University (Nanjing, China). For the tumor xenograft assay, 3×10^6 MDA-MB-231 cells were suspended in 200 μL PBS and subcutaneously injected into the right flank of the mice. When the tumors reached approximately 100 mm^3, the tumor-bearing mice were randomly divided into four groups. Then compound **7** (25mg/kg or 50mg/kg) and BPTES (25 mg/kg) were intraperitoneally administered every three days. After four weeks, all of the mice were euthanized. Then, the tumors and visceral organs of each group were collected and fixed in 4% paraformaldehyde. All animal experimental procedures followed the National Institutes of Health guide for the care and use of laboratory animals and were performed in accordance with protocols approved by the Institutional Animal Care and Use Committee (IACUC) of China Pharmaceutical University Experimental Animal Center.

4.11. Prediction of logP values

The partition coefficients (logP) were predicted with the Molinspiration Cheminformatics Software. The logP values were calculated by the methodology developed by Molinspiration as a sum of fragment-based contributions and correction factors. Method is very robust and is able to process practically all organic and most organometallic molecules.

Acknowledgements

This work was supported by the National Natural Science Foundation of China (No. 81872983), the Natural Science Foundation of Jiangsu Province (BK20181329) and the Drug Innovation Major Project (2018ZX09711-001-007).

References

[1] A. Wolf, S. Agnihotri, A. Guha, Targeting metabolic remodeling in glioblastoma multiforme, Oncotarget. 1 (2010) 552-562.

[2] M.G. Vander Heiden, L.C. Cantley, C.B. Thompson, Understanding the Warburg effect: the metabolic requirements of cell proliferation, Science. 3 (2009) 1029-1033.

[3] W.H. Koppenol, P.L. Bounds, C.V. Dang, Otto Warburg's contributions to current concepts of cancer metabolism, Nat. Rev. Cancer. 11 (2011) 325-337.

[4] J.W. Erickson, R.A. Cerione, Glutaminase: a hot spot for regulation of cancer cell metabolism? Oncotarget. 1 (2010) 734-740.

[5] P. Koppula, Y. Zhang, L. Zhuang, B. Gan, Amino acid transporter SLC7A11/xCT at the crossroads of regulating redox homeostasis and nutrient dependency of cancer, Cancer. Commun. 38 (2018) 12-25.

[6] D. Botman, W. Tigchelaar, C.J. Van Noorden, Determination of glutamate dehydrogenase activity and its kinetics in mouse tissues using metabolic mapping (quantitative enzyme histochemistry), Histochem. Cytochem. 62 (2014) 802-812.

[7] A. Le, A.N. Lane, M. Hamaker, S. Bose, A. Gouw, J. Barbi, T. Tsukamoto, C.J. Rojas, B.S. Slusher, H. Zhang, L.J. Zimmerman, D.C. Liebler, R.J. Slebos, P.K. Lorkiewicz, R.M. Higashi, T.W. Fan, C.V. Dang, Glucose-independent glutamine metabolism via TCA cycling for proliferation and survival in B cells, Cell Metab. 15 (2012) 110-121.

[8] W.P. Katt, R.A. Cerione, Glutaminase regulation in cancer cells: a druggable chain of events. Drug Discovery Today. 19 (2014) 450- 457.

[9] J.B. Wang, J.W. Erickson, R. Fuji, S. Ramachandran, P. Gao, R. Dinavahi, K.F. Wilson, A.L. Ambrosio, S.M. Dias, C.V. Dang, R.A. Cerione, Targeting mitochondrial glutaminase activity inhibits oncogenic transformation, Cancer Cell. 18 (2010) 207-219.

[10] M.J. Seltzer, B.D. Bennett, A.D. Joshi, P. Gao, A.G. Thomas, D.V. Ferraris, T. Tsukamoto, C.J. Rojas, B.S. Slusher, J.D. Rabinowitz, C.V. Dang, G.J. Riggins, Inhibition of glutaminase preferentially slows growth of glioma cells with mutant IDH1, Cancer Res. 70 (2010) 8981-8987.

[11] T. Cheng, J. Sudderth, C. Yang, A.R. Mullen, E.S. Jin, J.M. Mates, Pyruvate carboxylase is required for glutamine-independent growth of tumor cells, Proc. Natl. Acad. Sci. USA. 108 (2011) 8674-8679.

[12] A.P. Van Den Heuvel, J. Jing, R.F. Wooster, K.E. Bachman, Analysis of glutamine dependency in non-small cell lung cancer: GLS1 splice variant GAC is essential for cancer cell growth, Cancer. Biol. Ther. 13 (2012) 1185-1194.

[13] J. Son, C.A. Lyssiotis, H. Ying, X. Wang, S. Hua, M. Ligorio, Glutamine supports pancreatic cancer growth through a KRAS-regulated metabolic pathway, Nature. 496 (2013) 101-105.

[14] P.A. Gameiro, J. Yang, A.M. Metelo, R. Perez-Carro, R. Baker, Z. Wang, In vivo HIF-mediated reductive carboxylation is regulated bycitrate levels and sensitizes VHL-deficient cells to glutamine deprivation, Cell Metab. 17 (2013) 372-385.

[15] A. Cassago, A.P. Ferreira, I.M. Ferreira, C. Fornezari, E.R. Gomes, K.S. Greene, Mitochondrial localization and structure-based phosphate activation mechanism of glutaminase C with implications for cancer metabolism, Proc. Natl. Acad. Sci. USA. 109 (2012) 1092-1097.

[16] L.A. Timmerman, T. Holton, M. Yuneva, R.J. Louie, M. Padro, A. Daemen, Glutamine sensitivity analysis identifies the xCT Antiporter as a common triple-negative breast tumor therapeutic target, Cancer Cell. 24 (2013) 450-465.

[17] H.N. Kung, J.R. Marks, J.T. Chi, Glutamine synthetase is a genetic determinant of cell type-specific glutamine independence in breast epithelia, PLoS Genet. 7 (2011) e1002229.

[18] C. Kim, R. Gao, E. Sei, R. Brandt, J. Hartman, T. Hatschek, N. Crosetto, T. Foukakis, N.E.Navin, Chemoresistance evolution in triple-negative breast cancer delineated by single-cell sequencing, Cell. 173 (2018) 879-893.

[19] J.X. He, T.H. Peng, Y.B. Peng, L.L. Ai, Z.Y. Deng, X.Q. Wang, W.H. Tan, Molecularly Engineering Triptolide with Aptamers for High Specificity and Cytotoxicity for Triple-Negative Breast Cancer, J. Am. Chem. Soc. 142 (2020) 2699-2703.

[20] L. Zhang, L.L. Fu, S.Y. Zhang, J. Zhang, Y.Q. Zhao, Y.X. Zheng, G. He, S.Y. Yang, L. Ouyang, B. Liu, Discovery of a small molecule targeting ULK1- modulated cell death of triple negative breast cancer in vitro and in vivo, Chem. Sci. 8 (2017) 2687-2701.

[21] G.J. Yang W.H. Wang, S.W.F. Mok, C. Wu, B.Y.K. Law, X.M. Miao, K.J. Wu, H.J. Zhong, C.Y. Wong, V.K.W. Wong, D.L. Ma, C.H. Leung, SelectiveInhibition of Lysine-Specific Demethylase 5A (KDM5A)Using aRhodium(III) Complex for Triple-NegativeBreast CancerTherap, Angew. Chem. Int. Ed. 57 (2018) 13091-13095.

[22] W.D. Zhang, W.Y. Yu, G.P. Cai, J.W. Zhu, C. Zhang, S.S. Li, J.P. Guo, G.P. Yin, C. Chen, L.Y. Kong, A new synthetic derivative of cryptotanshinone KYZ3 as STAT3 inhibitor for triple-negative breast cancer therapy, Cell Death and Disease. 9 (2018) 1098-1109.

[23] M.I. Gross, S.D. Demo, J.B. Dennison, L. Chen, T. Chernov-Rogan, B. Goyal, J.R. Janes, G.J. Laidig, E.R. Lewis, J. Li, A.L. Mackinnon, F. Parlati, M.L. Rodriguez, P.J. Shwonek, E.B. Sjogren, T.F. Stanton, T. Wang, J. Yang, F. Zhao, M.K. Bennett, Antitumor activity of the glutaminase inhibitor CB-839 in triple-negative breast cancer. Mol. Cancer Ther. 2014, 13, 890-901.

[24] K. Thangavelu, C.Q. Pan, T. Karlberg, G. Balaji, M. Uttamchandani, V. Suresh, H. Schuler, B.C. Low, J. Sivaraman, Structural basis for the allosteric inhibitory mechanism of human kidney-type glutaminase (KGA) and its regulation by Raf-Mek-Erk signaling in cancer cell metabolism, Proc. Natl. Acad. Sci. USA. 109 (2012) 7705-7710.

[25] S. Ramachandran, C.Q. Pan, S.C. Zimmermann, B. Duvall, T. Tsukamoto, B.C. Low, Sivaraman J. Structural basis for exploring the allosteric inhibition of human kidney type glutaminase, Oncotarget. 7 (2016) 57943-57954.

[26] K. Thangavelu, Q.Y. Chong, B.C. Low, Sivaraman J. Structural basis for the active site inhibition mechanism of human kidney-type glutaminase (KGA), Sci Rep. 4 (2014) 3827-3833.

[27] R. Catane, D.D. Von Hoff, D.L. Glaubiger, F.M. Muggia, Azaserine, DON, and azotomycin: three diazo analogs of L-glutamine with clinical antitumor activity, Cancer Treat Rep. 63 (1979) 1033-1038.

[28] T.K. Yeh, C.C. Kuo, Y.Z. Lee, Design, Synthesis, and Evaluation of Thiazolidine-2,4-dione. Derivatives as a Novel Class of Glutaminase Inhibitors, J. Med. Chem. 60 (2017) 5599-5612.

[29] Z. Chen, D. Li, N. Xu, Novel 1,3,4-Selenadiazole-Containing Kidney-Type Glutaminase Inhibitors Showed Improved Cellular Uptake and Antitumor Activity, J. Med. Chem. 62 (2019) 589-603.

[30] M.R.V. Finlay, M. Anderton, A. Bailey, Discovery of a Thiadiazole-Pyridazine Based Allosteric Glutaminase 1 Inhibitor Series That Demonstrates Oral Bioavailability and Activity in Tumor Xenograft Models, J. Med. Chem. 62 (2019) 6540-6560.

[31] N. Jacque, A.M. Ronchetti, C. Larrue, G. Meunier, R. Birsen, L. Willems, E. Saland, J. Decroocq, T.T. Maciel, M. Lambert, L. Poulain, M.A. Hospital, P. Sujobert, Targeting glutaminolysis has antileukemic activity in acute myeloid leukemia and synergizes with BCL-2 inhibition, Blood. 126 (2015) 1346-1356.

[32] D.J. Newman, G.M. Cragg, Natural Products as Sources of New Drugs from 1981 to 2014, J. Nat. Prod. 79 (2016)629-661.

[33] T. Ma, W.N. Zhang, L. Yang, C. Zhang, R. Lin, S.M. Shan, M.D. Zhu, J.G. Luo, L.Y. Kong, Cytotoxic withanolides from Physalis angulata var. villosa and the apoptosis-inducing effect via ROS generation and the activation of MAPK in human osteosarcoma cells, RSC Advances. 6 (2016) 53089-53100.

[34] X.M. Xu, Y.Z. Guan, S.M. Shan, J.G. Luo, L.Y. Kong, Withaphysalin-type withanolides from Physalis minima, Phytochemistry Letters. 15 (2016) 1-6.

[35] C.Y. Zhang, J.G. Luo, R.H. Liu, R. Lin, M.H. Yang, L.Y. Kong. ^{1}H NMR spectroscopy-guided isolation of new sucrose esters from Physalis alkekengi var. franchetii and their antibacterial activity, Fitoterapia. 114 (2016) 138-143.

[36] Y.Z. Guan, S.M. Shan, W. Zhang, J.G. Luo, L.Y. Kong, Withanolides from Physalis minima and their inhibitory effects on nitric oxide production. Steroids. 2014, 82, 38-43.

[37] R. Lin, Y.Z. Guan, R.J. Li, X.M. Xu, J.G. Luo, L.Y. Kong, 13,14-seco-Withanolides from Physalis minima with Potential Anti-inflammatory Activity, Chemistry & Biodiversity. 13 (2016) 884-890.

[38] R.A. Shapiro, V.M. Clark, N.P. Curthoys, Inactivation of rat renal phosphate-dependent glutaminase with 6-diazo-5-oxo-L-norleucine. Evidence for interaction at the glutamine binding site, J. Biol. Chem. 254 (1979) 2835-2838.

[39] R.A. Shapiro, V.M. Clark, N.P. Curthoys, Covalent interaction of L-2-amino-4-oxo-5-chloropentanoic acid with rat renal phosphate-dependent glutaminase. Evidence for a specific glutamate binding site and of subunit heterogeneity, J. Biol. Chem. 253 (1978) 7086-7090.

[40] M.O. Yuneva, T.W. Fan, T.D. Allen, R.M. Higashi, D.V. Ferraris, T. Tsukamoto, J.M.

Mates, F.J. Alonso, C. Wang, Y. Seo, X. Chen, J.M. Bishop, The metabolic profile of tumors depends on both the responsible genetic lesion and tissue type, Cell Metab. 15 (2012) 157-170.

[41] R.W. Newcomb, M. Newocmb, Selective Inhibition of Glutaminase by Bis-Thiadiazoles. US6451828B1. Sep. 17, 2002.

[42] M.M. Robinson, S.J. McBryant, T. Tsukamoto, C. Rojas, D.V. Ferraris, S.K. Hamilton, J.C. Hansen, N.P. Curthoys, Novel mechanism of inhibition of rat kidney-type glutaminase bybis-2-(5-phenylacetamido-1,2,4-thiadiazol-2-yl)ethyl sulfide (BPTES), Biochem. J. 406 (2007) 407-414.

[43] K. Shukla, D.V. Ferraris, A.G. Thomas, M. Stathis, B. Duvall, G. Delahanty, J. Alt, R. Rais, C. Rojas, P. Gao, Y. Xiang, C. Dang, V.; Slusher, B. S.; Tsukamoto, T. Design, synthesis, and pharmacological evaluation of bis-2-(5-phenylacetamido-1,2,4-thiadiazol-2-yl)ethyl sulfide 3 (BPTES) analogs as glutaminase inhibitors, J. Med. Chem. 55 (2012) 10551-10563.

[44] S.C. Zimmermann, E.F. Wolf, A. Luu, A.G. Thomas, M. Stathis, B. Poore, C. Nguyen, A. Lee, C. Rojas, B.S. Slusher, Tsukamoto, T. Allosteric glutaminase inhibitors based on a 1,4-di(5-amino-1,3,4-thiadiazol-2-yl)butane scaffold, Acs Med. Chem. Lett. 7 (2016) 520-524.

[45] X.M. Xu, Y.Z. Guan, S.M. Shan, J.G. Luo, L.Y. Kong, Withaphysalin-type withanolides from Physalis minima, Phytochemistry Letters. 15 (2016) 1-6.

[46] Y.M. Xu, A.D. Brooks, E.M.K. Wijeratne, C.J. Henrich, P. Tewary, T.J. Sayers, A.A.L. Gunatilaka, 17β-Hydroxywithanolides as Sensitizers of Renal Carcinoma Cells to

Tumor Necrosis Factor-α Related Apoptosis Inducing Ligand (TRAIL) Mediated Apoptosis: Structure-Activity Relationships. J. Med. Chem. 60 (2017) 3039-3051.

[47] K. Jing, K.S. Song, S. Shin, N. Kim, S. Jeong, H.R. Oh, J.H. Park, K.S. Seo, J.Y. Heo, J. Han, J.I. Park, C. Han, T. Wu, G.R. Kweon, S.K. Park, W.H. Yoon, B.D. Hwang, K. Lim, Docosahexaenoic acid induces autophagy through p53/AMPK/mTOR signaling and promotes apoptosis in human cancer cells harboring wild-type p53, Autophagy. 7 (2011) 1348-1358.

[48] F. Weinberg, R. Hamanaka, W.W. Wheaton, S. Weinberg, J. Joseph, M. Lopez, B. Kalyanaraman, G.M. Mutlu, G.R. Budinger, S.; Chandel, N. S. Mitochondrial Metabolism and ROS Generation are Essential for Kras-Mediated Tumorigenicity, Proc. Natl. Acad. Sci. USA. 107 (2010) 8788-8793.

[49] Hamanaka, R. B.; Chandel, N. S. Mitochondrial reactive oxygen species regulate cellular signaling and dictate biological outcomes. Trends Biochem. Sci. 2010, 35, 505-513.

[50] B.J. Altman, Z.E. Stine, C.V. Dang, From Krebs to clinic: glutamine metabolism to cancer therapy, Nat. Rev. Cancer. 16 (2016) 619-634.

[51] B. DeLaBarre, S. Gross, C. Fang, Y. Gao, A. Jha, F. Jiang, J.J. Song, W.T. Wei, J.B. Hurov, Full-length human glutaminase in complex with an allosteric inhibitor. Biochemistry. 2011, 50, 10764-10770.

[52] R. Wagner, J.T. Randolph, S.V. Patel, L. Nelson, M.A. Matulenko, R. Keddy, J.K. Pratt, D. Liu, A.C. Krueger, P.L. Donner, D.K. Hutchinson, C. Flentge, D. Betebenner, T. Rockway, C.J. Maring, T.I. Ng, P. Krishnan, T. Pilot-Matias, C. Collins, N. Panchal, T. Reisch, T. Dekhtyar, R. Mondal, D.F. Stolarik, Y. Gao, W. Gao, D.A. Beno, W.M. Kati, Highlights of the Structure Activity Relationships of Benzimidazole Linked Pyrrolidines

Leading to the Discovery of Pibrentasvir/ABT-530, J. Med. Chem. 61 (2018) 4052-4066.

Highlights

- 25 withangulatin A derivatives were designed and synthesized as GLS1 inhibitors.
- Compound **7** showed the most potent GLS1 inhibitory potency.
- Docking study elucidated the binding pattern of **7** in the allosteric pocket of GLS1.
- **7** was demonstrated to be a promising candidate agent for the treatment of TNBC.

Declaration of interests

☒ The authors declare that they have no known competing financial interests or personal relationships that could have appeared to influence the work reported in this paper.

☐The authors declare the following financial interests/personal relationships which may be considered as potential competing interests: